James Webb Space Telescope

NIRSpec IFU observations to study Ganymede's surface properties

Master Thesis

Ingmar Boshuizen

Delft University of Technology

TU Delft

James Webb Space Telescope

NIRSpec IFU observations to study Ganymede's surface properties

by

Ingmar Boshuizen

4662776

Supervisor:	Dr. Stéphanie Cazaux	
Thesis Committee:	Prof. Dr. Bert Vermeersen	Chair
	Dr. Jérôme Loicq	Examiner
Institution:	Delft University of Technology	

TU Delft

Preface

This thesis marks the end of my 6 year journey at the Aerospace faculty of the TU Delft. It has not always been easy, but I am proud to have completed the challenging program. Finishing my master's by working with James Webb data has been incredible, especially when realising that the design of the telescope began before I was even born. During my minor in Liverpool, my professors told me about the new space telescope that was about to be launched. I am glad that they waited a couple of years until I was ready to start analysing the data.

I have enjoyed working on this thesis project the past year and I would like to thank my supervisor Stéphanie Cazaux for making this project possible. All your help and guidance in this project, your enthusiasm, helping me in generating new ideas when I was not sure where the project was going, making time for me to meet often and always respond fast to mails was highly appreciated.

I would like to thank Dominique Bockelée-Morvan for being extremely helpful in the pipeline calibration process, which at times was a slight pain in the... Furthermore, I would like to thank Eric Quirico, Olivier Poch and Emmanuel Lellouch for sharing their opinions during meetings. It was an honour for me to be part of the ERS 1373 program and one of the highlights of my thesis was definetely the conference we had in Meudon in October. Thanks to Imke de Pater and Thierry Fouchet and the rest of the team for inviting me and special thanks to Thierry for the great organisation. I would also like to thank Guillermo Manuel Muñoz Caro and Bruno Escribano for making time for our montly IR meeting and making useful suggestions for my project.

I would like to thank my parents for giving me advice when I was facing tough decisions and I would like to thank my dad in particular for reading my thesis and literature study and providing useful feedback. I would like to thank Erika Rogers and Ted Hill for inviting me in Los Osos and arranging for me to host a talk at Cal Poly, San Luis Obispo. I would like to thank my roommates Adt, Connie, Dobert, Goose, Njits and Skuum for all our great adventures and for allowing me to relax besides working. I would also like to thank Fiene van de Graaf for improving my workspace at home. Finally, I would like to thank my amazing girlfriend Maartje for always being there for me and supporting me throughout my studies.

Abstract

Ganymede is a fascinating object, being the largest moon in the Solar system and the only known moon to generate its own magnetic field. Ganymede is a fully differentiated body consisting of an iron core, silicate mantle and an ice outer layer. Ganymede's surface consists of old, dark terrain that is heavily cratered and young, light terrain containing grooves similar to Europa. Below the surface, Ganymede hosts a salty ocean containing more water than present in Earth's oceans.

The crystallinity of water ice on Ganymede has been investigated using Near Infrared Mapping Spectrometer (NIMS) and Very Large Telescope (VLT) data. NIMS data is used to determine the crystallinity in the first micrometre layer of Ganymede's surface using the Fresnel reflection peaks at 3.1 and 3.2 μm. VLT data on the other hand has been used to investigate crystallinity at millimetre level using the 1.65 μm water absorption band.

In August 2022, the James Webb Space Telescope (JWST) observed Ganymede's leading and trailing hemisphere as part of the Early Release Science (ERS) program. This was designed to test JWST's capability of performing Solar System science and has the objective to map the distribution of CO_2, H_2O and organic material on the surface of Ganymede. Using the Near Infrared Spectrograph's (NIRSpec) observations, the crystallinity in the first micrometre layer of the entire surface of Ganymede is investigated. In order to do so, the following research question is defined.

How can variations in crystallinity of water ice be linked to energetic processes occurring on the surface of Ganymede?

In this research, the Fresnel reflection peak position at 3.1 μm is used as a measure of crystallinity. The Crystallinity Factor (CF) is obtained by taking a linear combination of the peak position of amorphous and crystalline water ice models. These models are defined using the Fresnel factor. Two trends are observed in the distribution of the CF. A latitudinal trend on the leading hemisphere is observed. Signatures of amorphous ice are found on the poles of the leading hemisphere, which makes sense as the flux is highest in this region. Ganymede's magnetic field protects the low latitude region from low energetic impacts, meaning that the ice is more crystalline in this region.

At both leading and trailing hemispheres, a longitudinal trend in CF is observed where crystallinity decreases over the course of a day on Ganymede. In order to explain this behaviour, the crystallisation and amorphisation time have to be known to see which process is dominant. Therefore, a model is made linking the crystallisation and amorphisation time to temperature. When using parameters of laboratory experiments, it is observed that the crystallisation process is the dominant process after approximately 130 K which is not in line with the observations. However, by extrapolating the laboratory conditions to the conditions on Ganymede's surface it is found that amorphisation due to ultraviolet (UV) irradiation could be the dominant process, also at high temperatures.

List of Figures

List of acronyms

A&A	Astronomy and Astrophysics
CF	Crystallinity Factor
CO_2	Carbon dioxide
ERS	Early Release Science
FITS	Flexible Image Transport System
H_2O	Water
IFU	Integral Field Unit
IR	InfraRed
JIRAM	Jovian InfraRed Auroral Mapper
JUICE	JUpiter Icy Moons Explorer
JWST	James Webb Space Telescope
MAJIS	Moons and Jupiter Imaging Spectrometer
MAST	Mikulski Archive for Space Telescopes
MIRI	Mid InfraRed Instrument
NIMS	Near Infrared Mapping Spectrometer
NIR	Near InfraRed
NIRSpec	Near InfraRed Spectrograph
SO_2	Sulfur dioxide
UV	UltraViolet
VLT	Very Large Telescope

Contents

1 Introduction

Being the largest moon in the Solar system, Ganymede is a unique moon. It is a differentiated body, consisting of an iron core, covered by a silicate mantle and topped by an ice outer layer (Anderson et al., 1996). Ganymede hosts a subsurface salty ocean on top of the silicate mantle (Kivelson et al., 2002). Furthermore, Ganymede is the only known moon to generate its own internal magnetic field (Kivelson et al., 1996).

The surface of Ganymede consists of two major terrain types. There is old (4 Gyr), dark terrain that covers approximately a third of the surface and younger (2 Gyr), light terrain covering the other two thirds. High resolution imaging by the Galileo spacecraft revealed that dark terrain consists of non ice material that accumulated on the surface (Patterson et al., 2009; Pappalardo et al., 2004). However, it is not yet known what this non ice material is exactly. The non ice component could consist of CO_2 (Hibbitts et al., 2003), SO_2, organic materials and sulfur bearing minerals (McCord et al., 1997; Prockter et al., 2000; Ligier et al., 2019). The presence of grooved terrain on the surface of Ganymede is seen as evidence of tectonic activity (Patterson et al., 2009) and flooded regions on the surface suggest cryovolconism (Kay and Head, 1999).

Reflectance spectra of water ice show emission peaks at 3.1 and 3.2 μm (Stephan et al., 2021). These Fresnel reflection peaks are caused by the reflection of grains at the surface of the reflecting body (Hansen, 2002). The shape of the Fresnel peaks depends on temperature, particle size and the crystallinity of water ice (Schmitt et al., 1998) and the peaks have been detected previously on Ganymede by the Galileo and Juno spacecraft (McCord et al., 1997; Mura et al., 2020). The shape and position of the Fresnel peaks give insight into the crystallinity of water ice. This is an important parameter on icy bodies as it is an indicator of the energetic processes occurring on the surface. Crystallinity is influenced by temperature, particle bombardment, water vapor deposition and cryovolcanic activity (Berdis et al., 2022).

Hansen and McCord (2004) used the detected Fresnel peaks in NIMS spectra to determine the crystallinity of water ice on Ganymede. In this research it was determined that amorphous and crystalline ice are both common in the first μm layer of the surface of Ganymede. Using the 1.65 μm water band, spectra obtained with the Very Large Telescope (VLT) suggest that ice is mostly crystalline at millimetres beneath the surface (Ligier et al., 2019). This is due to the fact that low energy impacts are already absorbed in this region. Furthermore, the observations in the 1.4-2.5 μm region have reported a latitudinal trend in amorphous ice, where ice becomes more amorphous at the poles of the leading hemisphere. It is also mentioned that amorphous ice is distributed homogeneously over the surface of Ganymede, whereas crystalline ice on the other hand is mostly present on the leading hemisphere and follows a similar distribution as the abundance of water ice in general.

After being launched successfully towards the Earth-Sun L2 point during Christmas 2021, the James Webb Space Telescope (JWST) observed Ganymede's leading and trailing hemisphere in August 2022. These observations are part of the Early Release Science (ERS) 1373 program, with the goal to perform

observations of the Jovian System as a demonstration of JWST's capability for Solar System science. Both NIRSpec and MIRI observations were done to complement previous near-infrared observations and to extend this knowledge to the infrared. Aims of the observations are to map the distribution of CO_2, H_2O and organic material on the surface of Ganymede (Bockelée-Morvan et al. in prep). In the NIRSpec spectra an H_2O_2 signature at 3.5 μm was detected, similar to the one on Europa (Trumbo et al., 2023).

In order to structure the research concerning JWST NIRSpec observations, four research questions are established.

1. How can variations in crystallinity of water ice be linked to energetic processes occurring on the surface of Ganymede?
2. What can NIRSPec high resolving power observations reveal about CO_2 abundance in Ganymede's exosphere?
3. What can the CO_2 $\nu 3$ absorption band reveal about the state and distribution of CO_2 on Ganymede's surface?
4. Can NIRSpec's high resolving power observations gain more insight into the distribution of organic material on the surface of Ganymede?

The main focus of this thesis project concerns the first research question. The findings concerning this objective are presented in the form of a journal article which is shown in chapter 2. Next conclusions and recommendations for future work are given for all research objectives in section 3. In the appendices all the research that has been conducted during the thesis is presented, starting with data acquisition in appendix A. Then additional results concerning water ice, CO_2 and organics are presented in appendix B and finally the results are validated in appendix C.

2

Article

This chapter presents the main focus of the thesis in a paper format. The article 'The crystallinity of water ice on Ganymede' is written using the standard Astronomy and Astrophysics (A&A) template and guidelines.

Astronomy & Astrophysics manuscript no. output
June 21, 2023

The Crystallinity of Water Ice on Ganymede

JWST NIRSpec observations of the icy moon

I.T. Boshuizen

Delft University of Technology, Faculty of Aerospace Engineering, Kluyverweg 1, 2629 HS Delft
e-mail: ingmar.boshuizen@hotmail.com

June 21, 2023

ABSTRACT

Context. Ganymede is the largest moon in the Solar System and with its salty subsurface ocean and its own magnetic field, Ganymede is a unique moon. Its leading and trailing hemisphere have been observed by the James Webb Space Telescope's MIRI and NIRSpec instruments in August 2022 as part of the Early Release Science program, demonstrating JWST's capability of doing Solar System science.
Aims. Using NIRSpec observations of Ganymede's leading and trailing hemisphere, the crystallinity of water ice on the surface of Ganymede and the distribution of crystalline and amorphous ice can be determined. The crystallinity of water ice on Ganymede gives insight into energetic processes occurring on the surface of the icy moon.
Methods. The shape and location of the Fresnel peaks at 3.1 and 3.2 μm can be used to constrain the crystallinity of water ice. To obtain the crystallinity factor (CF) of water ice, the location of the 3.1 μm peak compared to amorphous and crystalline water ice is used as a crystallinity indicator.
Results. The observations show two trends in crystallinity: latitudinal and longitudinal. The North pole of the leading hemisphere shows the most signatures of amorphous ice due to the high flux of energetic particle in this region due to interaction with Jupiter's magnetosphere. Furthermore, it is observed that ice becomes more amorphous during the course of a day on Ganymede for both leading and trailing hemispheres.
Conclusions. The magnetic field of Ganymede is generally responsible for the latitudinal variations seen on the leading hemisphere. It protects the equatorial region from low energetic impacts and guides particles towards the poles, where the most significant fraction of amorphous ice are present. The longitudinal variations seem to be related to daily effects. UV irradiation of the surface of Ganymede is proposed to be the cause of amorphisation of water ice being a faster process than the crystallisation process.

Key words. JWST Solar System Science – NIRSpec – Ganymede – spectroscopy – water ice crystallinity

1. Introduction

Being the largest moon in the Solar system, Ganymede is a unique moon. It is a differentiated body, consisting of an iron core, covered by a silicate mantle and topped by an ice outer layer (Anderson et al. 1996). Ganymede hosts a subsurface salty ocean on top of the silicate mantle (Kivelson et al. 2002). Furthermore, Ganymede is the only known moon to generate its own internal magnetic field (Kivelson et al. 1996).

The surface of Ganymede consists of two major terrain types. There is old (4 Gyr), dark terrain that covers approximately a third of the surface and younger (2 Gyr), light terrain covering the other two thirds. High resolution imaging by the Galileo spacecraft revealed that dark terrain consists of non ice material that accumulated on the surface (Patterson et al. 2009; Pappalardo et al. 2004). However, it is not yet known what this non ice material is exactly. The non ice component could consist of CO_2 (Hibbitts et al. 2003), SO_2, organic materials and sulfur bearing minerals (McCord et al. 1997; Prockter et al. 2000; Ligier et al. 2019). The presence of grooved terrain on the surface of Ganymede is seen as evidence of tectonic activity (Patterson et al. 2009) and flooded regions on the surface suggest cryovolconism (Kay & Head 1999).

Reflectance spectra of water ice show emission peaks at 3.1 and 3.2 μm (Stephan et al. 2021). These Fresnel reflection peaks are caused by the reflection of grains at the surface of the reflecting body (Hansen 2002). The shape of the Fresnel peaks depends on temperature, particle size and the crystallinity of water ice (Schmitt et al. 1998) and the peaks have been detected previously on Ganymede by the Galileo and Juno spacecraft (McCord et al. 1997; Mura et al. 2020). The shape and position of the Fresnel peaks give insight into the crystallinity of water ice. This is an important parameter on icy bodies as it is an indicator of the energetic processes occurring on the surface. Crystallinity is influenced by temperature, particle bombardment, water vapor deposition and cryovolcanic activity (Berdis et al. 2022).

Hansen & McCord (2004) used the detected Fresnel peaks in NIMS spectra to determine the crystallinity of water ice on Ganymede. In this research it was determined that amorphous and crystalline ice are both common in the first μm layer of the surface of Ganymede. Using the 1.65 μm water band, spectra obtained with the Very Large Telescope (VLT) suggest that ice is mostly crystalline at millimetres beneath the surface (Ligier et al. 2019). This is due to the fact that low energy impacts are already absorbed in this region. Furthermore, the observations in the 1.4-2.5 μm region have reported a latitudinal trend in

amorphous ice, where ice becomes more amorphous at the poles of the leading hemisphere. It is also mentioned that amorphous ice is distributed homogeneously over the surface of Ganymede, whereas crystalline ice on the other hand is mostly present on the leading hemisphere and follows a similar distribution as the abundance of water ice in general.

After being launched successfully towards the Earth-Sun L2 point during Christmas 2021, the James Webb Space Telescope (JWST) observed Ganymede's leading and trailing hemisphere in August 2022. These observations are part of the Early Release Science (ERS) 1373 program, with the goal to perform observations of the Jovian System as a demonstration of JWST's capability for Solar System science. Both NIRSpec and MIRI observations were done to complement previous near-infrared observations and to extend this knowledge to the infrared. Aims of the observations are to map the distribution of CO_2, H_2O and organic material on the surface of Ganymede (Bockelée-Morvan et al. in prep). In the NIRSpec spectra an H_2O_2 signature at 3.5 μm was detected, similar to the one on Europa (Trumbo et al. 2023). With the JWST observations the global distribution of the crystallinity of water ice on the entire surface of Ganymede can be appreciated by using the Fresnel peaks band centre. The extent to which crystallinity changes with longitude and latitude can be linked to energetic processes on the surface.

In this paper, the data reduction is described in section 2. Then the methodology on how to obtain the crystallinity factor (CF) of water ice is presented in section 3, after which the results showing the distribution of amorphous and crystalline water ice over the surface of Ganymede are shown in section 4. The results are discussed in section 5 and the paper is concluded in section 6.

2. Observations and data reduction

For this research, use was made of leading and trailing hemisphere observations of the NIRSpec IFU on board the JWST. NIRSpec's IFU is capable of producing a reflectance spectrum of every pixel that it observes, making it very suitable to map the distribution of absorption features of its target. The observations were made on August 3 and August 7, 2022 for trailing (observation 28) and leading (observation 19) hemisphere respectively. Ganymede was observed for 40 minutes for both observations, using the G395H/F290LP disperser-filter combination. This results in high resolving power (R=2700) spectra in the 2.87-5.28 μm wavelength range. NIRSpec's IFU has a 3"× 3" FOV and samples Ganymede at 0.1" × 0.1", which is about 315 x 315 km locally. Both observations make use of a four-point dither, separated by 0.4" in order to average out bad pixels.

The incoming flux is detected by the two NIRSpec detectors in the focal plane array, nrs1 and nrs2. Due to a physical gap between the two detectors, the 4.0 - 4.15 μm range is excluded from the spectra. This is unfortunate since the gap makes it impossible to detect the SO_2 absorption band at 4.05 μm.

The data is reduced using the JWST pipeline version 1.9.4 in three stages. The first stage consists of the calwebb_detector1 module which is used for all JWST observations. In this stage of the pipeline, raw data is converted into uncalibrated slope images. These images are calibrated in the second stage of the pipeline using the calwebb_spec2 module. Furthermore, in this second stage a background subtraction and a flat field correction are done and the data is formatted in the World Coordinate System (WCS). Moreover, a flux calibration is done to convert the data to the desired units of MJy/sr. In the third and final stage, the calibrated images of the four dithers are combined into 3D data cubes using the calwebb_spec3 module. In the cube_build step of the third stage, use was made of the 'ifualign' coordinate system. This way, the cube is built in the detector frame rather than in sky coordinates to minimise artifacts forming in the spectra. An example of a reduced spectrum of the trailing hemisphere is shown in figure 1.

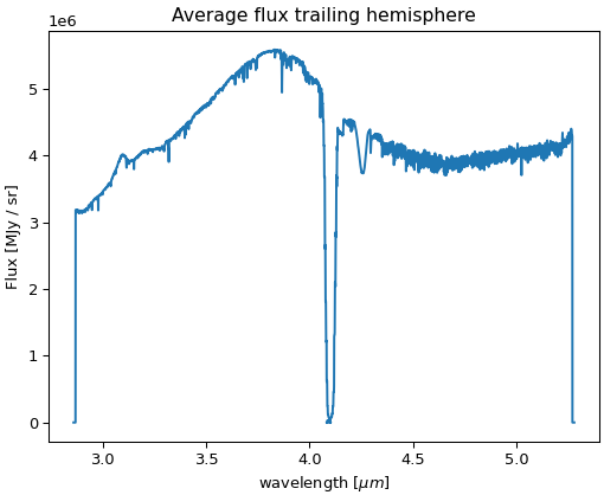

Fig. 1. Example of a reduced spectrum of the trailing hemisphere. Note the presence of the Solar lines.

In the observed wavelength range, the detected flux from Ganymede is dominated by reflected sunlight. Therefore, solar lines dominate the flux spectra and interfere with Ganymede's surface features as can be seen in figure 1. To fully assess Ganymede's features, the Solar flux needs to be removed from the spectra. This is done by converting the received flux to the radiance factor, I/F. Here, I is the flux of Ganymede and F is the Solar flux. The correction is done using a Solar spectrum of R.L. Kurucz [1] in the wavelength range of the NIRSpec observations. Since the Solar spectrum is in a Solar inertial reference frame, the signal is Doppler shifted when the light is detected at the JWST. In order to match the Solar lines of the spectrum with the JWST observations, two Doppler shifts have to be taken into account. The first shift takes the heliocentric velocity of Ganymede into account whereas the second shift accounts for Ganymede's velocity with respect to the JWST. It is found that an extra shift of 0.168 nm should be applied, to fully optimise the removal of Solar lines and to be able to optimally asses Ganymede's features. Finally, the Solar spectrum is converted to the same spatial resolution as the JWST observations and the Solar lines are removed.

3. Method

3.1. Fitting the Fresnel peak

To be able to extract features from the reflectance spectra, the Fresnel peaks are fitted by the sum of an order four polynomial and two Gaussians. This is needed since some spectra contain noise, especially near the limb due to the lower signal-to-noise. An example of a fit is shown in figure 2, using the spectrum

[1] http://kurucz.harvard.edu/sun.html

from pixel (17,16) near the equator of the leading hemisphere. Furthermore, the figure illustrates how the data is fitted by summing the Gaussians with a polynomial. The sum of squared residuals (SSR) equals $3.32 \cdot 10^{-5}$ for pixel (17,16). Moreover, all other pixels have a SSR of the same order of magnitude or smaller for the leading and trailing hemisphere. Compared to the order of magnitude of the data, the SSR is small and it has the same order of magnitude as the fits presented by Hansen & McCord (2004) in determining the CF. Therefore, the fits are deemed sufficient.

Once the data is fitted, the continuum can be defined and subtracted to define the peak positions. The polynomial displayed in figure 2 is not used for this. Even though it is needed to properly fit the data, it does not represent the true continuum. In Mastrapa et al. (2009) it can be seen that the broad water absorption band has its minimum at approximately 3 μm (see figure 10), which is not achieved by the polynomial. This is caused by the fact that the NIRSpec data starts at 2.87 μm, meaning that only part of the water band is available. For this research, a straight line stretching from 3-3.275 μm is deemed close enough to the real continuum similar to the research of Trumbo et al. (2023) and Bockelée-Morvan et al. (in prep). Finally, this line is subtracted from the fit.

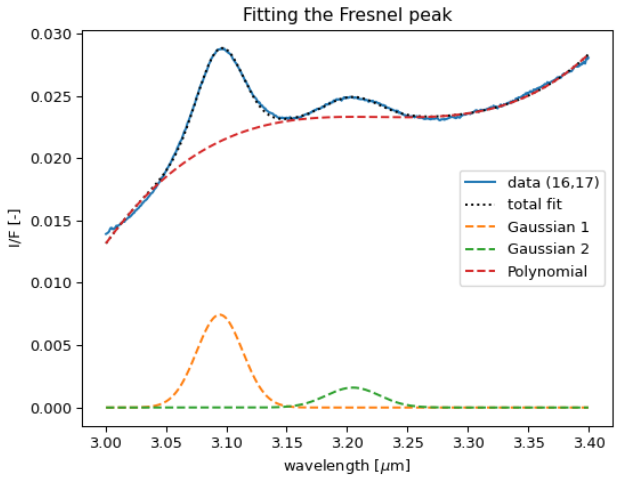

Fig. 2. Example of fitting the Fresnel peak using the sum of two Gaussians and an order four polynomial. The data is from pixel (17,16), located near the equator on the leading hemisphere.

3.2. Calculating the Crystallinity Factor

In order to determine the crystallinity of water ice using the Fresnel peaks, an ice model is needed to compare the data to. For this research, use was made of the Fresnel factor (R) as defined by Vašíček & Watney-Kaczér (1960). The Fresnel factor is calculated using equation 1. It can be seen that the Fresnel factor is a function of the optical constants (n and k) of water ice. For this research, the optical constants obtained by Mastrapa et al. (2009) in the desired wavelength range are used.

$$R = \frac{(n-1)^2 + k^2}{(n+1)^2 + k^2} \tag{1}$$

The Fresnel factor is obtained for both crystalline (R_c) and amorphous (R_a) ice. The CF is calculated by taking a linear combination of the peak position of the amorphous and crystalline Fresnel factor functions as shown in equation 2 and visualised in figure 3. In the equation, $max(R_{JWST})$ is the band position of the first Fresnel peak detected by the JWST. This is represented by the blue, dotted line in figure 3. The position of the first peak is determined by taking the maximum of the fit in the 3 - 3.15 μm range, after the continuum is subtracted.

$$max(R_{JWST}) = CF \cdot max(R_C) + (1 - CF) \cdot max(R_A) \tag{2}$$

The optical constants of water vary with temperature. Furthermore, the surface temperature of Ganymede is not constant as it is colder at the poles than near the equator. The average surface temperature on Ganymede is about 110K (Vance et al. 2014). However, when calculating the crystallinity factor the most extreme case is taken within the range of temperatures on Ganymede. Therefore, the optical constants of the highest available temperature are taken from Mastrapa et al. (2009) (150K for crystalline and 120K for amorphous ice). Taking the optical constants at lower temperatures will affect the absolute value of the CF. However, the distribution and behaviour of the CF over the surface of Ganymede, presented in subsection 4.2, will not change.

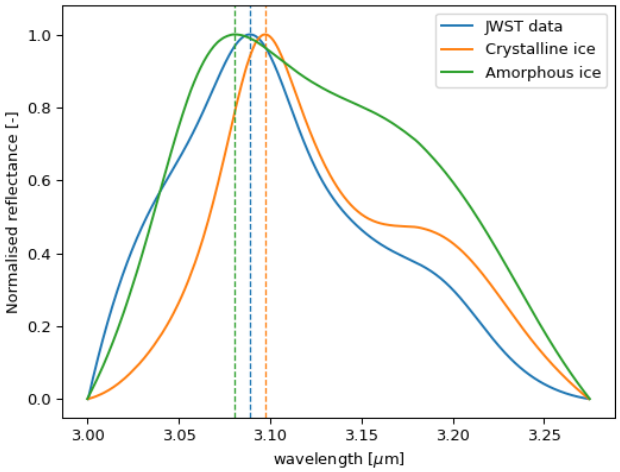

Fig. 3. Example of the determination of the CF, using a linear combination of the peak position of crystalline ice at 150K (orange) and amorphous ice at 120K (green).

4. Results

4.1. The Fresnel peaks for different latitudes

Figure 4 shows the Fresnel peaks for both leading and trailing hemispheres as observed by NIRSpec's IFU for the indicated range of latitudes. From the figure, a clear peak can be seen at 3.1 μm for both leading and trailing hemisphere. The second peak at 3.2 μm is more obvious for the leading hemisphere but can be observed on the trailing side as well. When looking at the different latitudes, it can be seen that there is a slight blueshift of the Fresnel peak at the leading North pole suggesting that water ice is more amorphous than at lower latitudes. Furthermore, the Fresnel peak is more flattened at the poles.

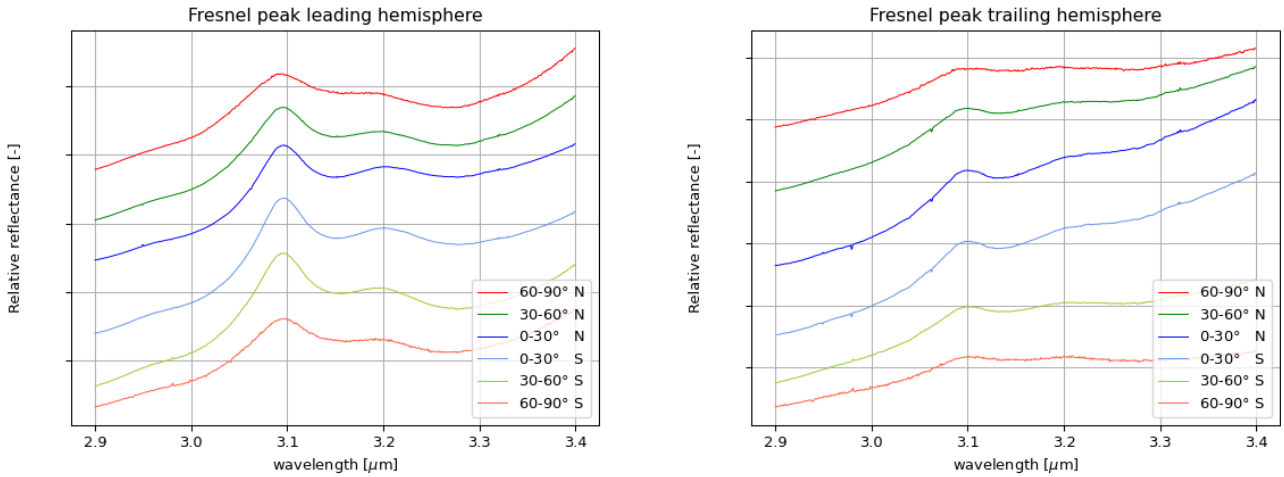

Fig. 4. Latitudinal variations in the Fresnel peaks observed by NIRSpec for Ganymede's leading (left) and trailing (right) hemisphere. The flux is averaged for pixels in a certain range of latitudes according to the legend.

4.2. The distribution of the crystallinity factor

The distribution of the CF, along with the peak position of the two Fresnel peaks for leading and trailing hemispheres are shown in figure 5. From the figure, both latitudinal and longitudinal variations in CF are visible. The latitudinal variations are mostly visible on the leading hemisphere. The poles have more amorphous ice than the equatorial region, while the most signatures of amorphous ice are visible on the North pole. Note that all the ice mostly tends towards crystalline as the CF is above 0.5 everywhere. The latitudinal variations of amorphous ice are in agreement with research by Ligier et al. (2019) in the 1.05 - 2.50 μm range.

In the maps of the leading hemisphere, the 92 km diameter Tros crater can be seen on the leading hemisphere on the top right of figure 5A and C, having a slightly different CF and Fresnel peak position than its surroundings (Ravine et al. 2022). This could be caused by a temperature effect. The bright crater has a higher albedo than the surrounding terrain, meaning that the surface temperature is lower (Brown et al. 2023). This implies a longer crystallisation time in the crater thus showing more amorphous signatures.

For both leading and trailing hemispheres, a change in CF and Fresnel peak position can be observed over different longitudes. At higher longitudes, ice is more crystalline than at lower longitudes for both hemispheres. This implies that the crystallinity of water ice changes during a day on Ganymede.

4.3. The area of the Fresnel peaks

One of the major differences between the Fresnel peaks of amorphous and crystalline ice is the presence of a second peak at 3.2 μm for crystalline ice, as can be seen from figure 3. For amorphous ice this peak is much less distinguishable than for crystalline ice, implying that the peak might be a good indicator for the crystallinity of the ice (Stephan et al. 2021). Figure 6 shows the area of the first and second Fresnel peak for the leading and trailing hemisphere. It can be seen that the first and second Fresnel peak show similar distributions for both hemispheres. From the figure it can also be seen that the area of the Fresnel peaks is correlated with the bond albedo of Ganymede. This is visualised in figure 7 in which the first peak area (left panels) and second peak area (right panels) are shown versus the bond albedo. This could be explained by the fact that dark terrain (with low albedo) contains less water ice than light terrain. Furthermore, the maps of the Fresnel peak area are similar to the general water ice distribution as derived by Trumbo et al. (2023). This makes sense as the area of the Fresnel peak is generally an indication of the abundance of water ice (Bockelée-Morvan in prep.). For the trailing hemisphere the correlation with albedo is visible, as shown in figure 7 but seems to have a few outliers.

The area of the first and second Fresnel peak exhibit similar distributions. However, the areas do not correlate with the observed CF. This shows that the area is not suitable to use as an indication of the crystallinity of the water ice, but rather as an indication of the abundance of water ice. The distribution of the water ice in the maps is in agreement with previous studies (Ligier et al. 2019; Hansen & McCord 2004; Trumbo et al. 2023).

5. Discussion

There are several processes that can cause variations in the properties of water ice. For example, the surface temperature, impacts by (micro)meteorites (Stephan et al. 2020, 2021) and impacts of energetic particles (Plainaki et al. 2022). Naturally, the way in which these phenomena affect the surface of Ganymede depends on Ganymede's orbital position and the flux in the Jovian magnetosphere (Paranicas et al. 2018).

Amorphous ice can be present on Ganymede if water vapor is deposited at the surface at low temperatures (Klinger 1985). However, for temperatures typical to Ganymede's ice would crystallise to cubic crystalline ice (I_c) in a matter of hours if there are no impacts or internal heat sources (Famá et al. 2009). Therefore, the presence of amorphous ice is mostly linked to the impacts of particles from space, weathering with UV photons, or charged, energetic particles from the magnetosphere of Jupiter. This section will link the particle impacts and UV irradiation to the observed latitudinal and longitudinal variations.

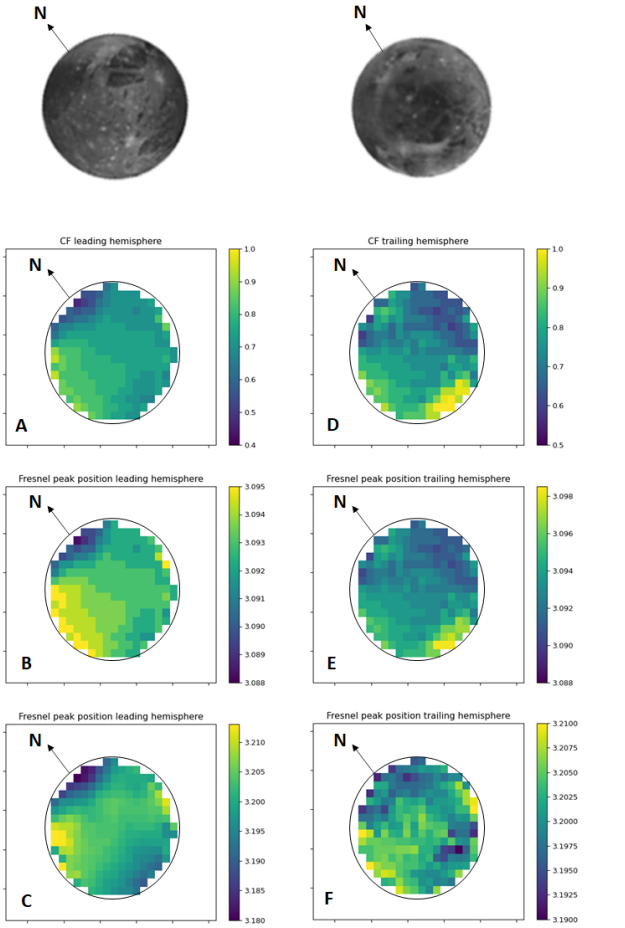

Fig. 5. Leading (top left) and trailing (top right) hemisphere of Ganymede derived by De Kleer et al. (2021). CF of leading (A) and trailing (D) hemisphere, where a CF of 0 represents amorphous ice and a CF of 1 crystalline ice. The middle and bottom row show the peak position of the first and second Fresnel peak respectively for the leading (B and C) and trailing (E and F) hemisphere. North is indicated by the arrow.

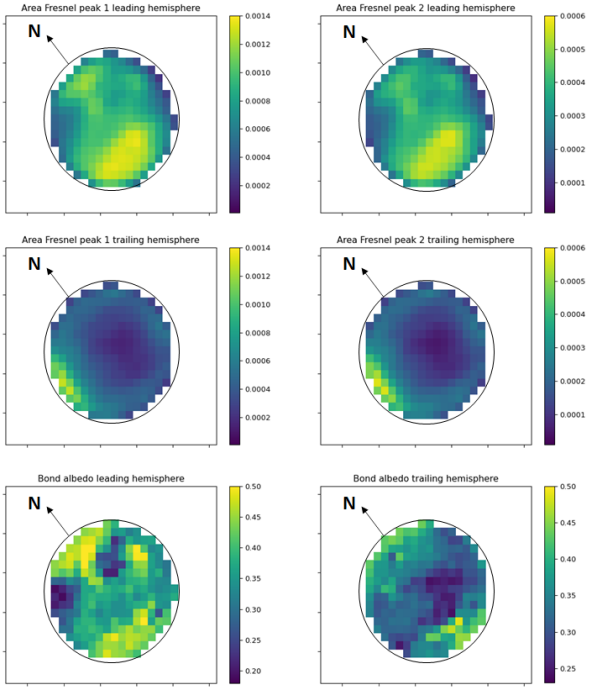

Fig. 6. The area of the first (top) and second (middle) Fresnel peak is shown for leading (left) and trailing (right) hemisphere. Furthermore, maps of the bond albedo for leading (bottom left) and trailing (bottom right) hemisphere, derived from De Kleer et al. (2021) are shown. The mean albedo of the surface area of every NIRSpec IFU pixel is taken.

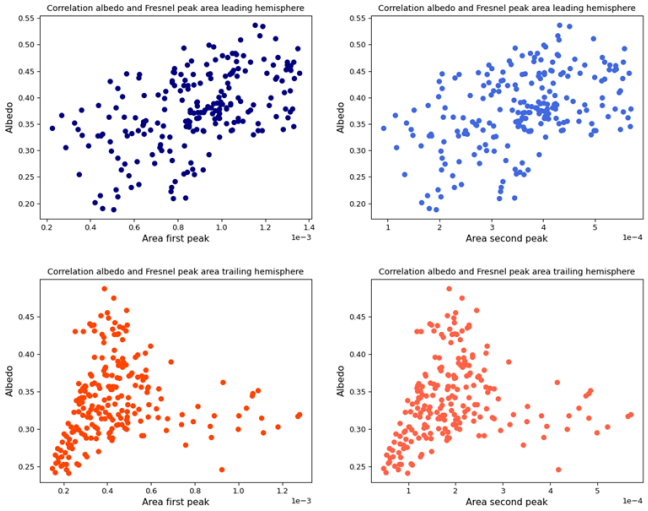

Fig. 7. Correlation between the area of the first and second Fresnel peak and the bond albedo for leading and trailing hemisphere.

5.1. Latitudinal variations

In figure 5 latitudinal variations in the crystallinity of water ice are observed. This especially holds for the leading hemisphere and is in agreement to previous research by Ligier et al. (2019). Ganymede's magnetic field plays a major role in the distribution of amorphous ice on its surface. Ganymede's magnetic field is sufficiently strong to create a small magnetosphere around the moon, shielding the equatorial region of the leading hemisphere from low energy impacts (Poppe et al. 2018). Instead, particles are guided towards the poles by the closed field lines of Ganymede's magnetic field. Therefore, the poles on the leading hemisphere are subject to the highest amount of ion flux (Poppe et al. 2018). Lab experiments have shown the impact of radiation on crystalline ice. In Baragiola et al. (2005), the shape of a crystalline Fresnel peak changes (see figure 3) to the amorphous reflection peak with increasing amounts of radiation. Due to the high flux at the poles of the leading hemisphere, the abundance of amorphous ice is highest here. Furthermore, the poles are colder than the equatorial region which implies that the crystallisation time is longest in these regions. This explains why the poles have the largest traces of amorphous ice.

On the trailing hemisphere, latitudinal variations are less distinguishable. On the North pole the ice seems more crystalline than the surrounding terrain and the South pole also shows traces of crystalline ice. This is direct evidence that the leading and trailing hemisphere of Ganymede are exposed to different weathering conditions. Jupiter's plasma sheet is known to almost co-rotate with the Galilean satellites. However, the plasma catches up with the moons in their orbits. Therefore, low energy (energy below 10 keV) ions and electrons are known to

mostly impact the trailing hemisphere (Johnson et al. 2004).

The bombardment of energetic particles from the Jovian plasma sheet leads to the ejection of among others water ice. The amount of sputtering of H_2O molecules not only depends on the surface location, but also Ganymede's orbital position (Plainaki et al. 2022; Poppe et al. 2018). Simulations of Leblanc et al. (2017) show that sputtering is maximum at a phase angle of 270°. This implies that the crystallinity of the surface of Ganymede is affected by its orbital position.

To summarise, amorphous ice signatures are mostly visible on the poles of the leading hemisphere due to the impacts of energetic particles. Below the close field lines no latitudinal variations are observed, since these regions are shielded from low energetic particles by the magnetic field. On the trailing hemisphere, a latitudinal trend is not visible indicating that the leading and trailing hemisphere are bound to different processes.

5.2. Longitudinal variations

The CF evolves as a function of longitude for both leading and trailing hemisphere, as can be seen in figure 5. It can be seen that the CF is higher (i.e. leaning more towards crystalline ice) at the morning limb and decreases during the course of a day on Ganymede. In order to understand this behaviour, two processes can be considered. Water ice crystallises at a certain rate, depending on the temperature (Schmitt et al. 1989; Faure et al. 2015). Amorphisation of water ice occurs when the ice is impacted by UV radiation (Leto & Baratta 2003) or energetic particles (Stephan et al. 2020; Plainaki et al. 2022). The degree of amorphisation of water ice directly depends on the balance between crystalisation rate (due to temperature) and amorphisation rate (due to energetic processes).

Research from Leblanc et al. (2017) and Bockelée-Morvan et al. (in prep.) show that the surface temperature of Ganymede ranges between 80 and 160 K approximately, depending on the local time. During a day on Ganymede the surface warms up, as it receives Solar radiation. This could cause water ice to crystallise. For example, at 135K the crystallisation process would take 2 hours (Mitchell et al. 2017) and as temperature increases the process will be exponentially faster (Schmitt et al. 1989; Faure et al. 2015). The observations however, do not show a crystallisation process as the CF decreases from the morning to the evening limb, as visualised in figure 8. In order to explain the observations, the amorphisation process has to be taken into account.

The morning limb of both leading and trailing hemisphere shows signs of crystalline ice. During the cold night on Ganymede, water from below the surface (where it is warmer) vaporises and freezes onto the surface (Bockelée-Morvan et al. in prep.). Water vapor has been detected by the Hubble Space Telescope (HST) in Ganymede's exosphere (Roth et al. 2021). During a day on Ganymede, the water ice is processed by UV radiation causing the ice to amorphise. However, research by Kouchi & Kuroda (1990, 1991) showed that cubic crystalline ice (Ic) can only become amorphous due to UV radiation at a temperature below 70K. This was confirmed in research by Leto & Baratta (2003); Tachibana et al. (2017); Kouchi et al. (2021) where Ic was amorphised at 16 K, 60 K and below 70 K respectively.

In order to be able to compare the conditions on Ganymede to the lab, a model was developed which is explained in appendix A. The aim of this model is to use the rates of ice amorphisation and crystallisation derived from laboratory experiments and apply them to the conditions on Ganymede. The amorphisation rate is dependent on the flux of UV photons (F), number of molecules per cm^2 (n), penetration depth of UV photons (d), equal to 0.1 μm (Kouchi et al. 2021) and the absorption coefficient (a). This coefficient in turn depends on the imaginary part of the optical constant (k) and wavelength (λ) (Leto & Baratta 2003). In laboratory experiments, Ly-α photons are commonly used with an energy of 10.2 eV resulting in a constant absorption coefficient (Leto & Baratta 2003). On Ganymede, the photons impinging the surface have a flux following a distribution in energy that follows a Solar black body distribution. In order to amorphise the water ice on Ganymede, high energetic photons are required with an energy of at least 6 eV (i.e. $\lambda < 207$ nm (Cooper et al. 2001).

Figure 8 shows how the CF changes due to amorphisation and crystallisation of water ice. When both processes are considered, it can be seen that amorphisation is dominant at low temperatures, whereas crystallisation becomes more dominant at about 130 K. The figure also presents the model when a higher value for the absorption coefficient is considered than the one derived in lab experiments, which causes the CF to shift upwards due to a longer amorphisation time.

The crystallisation process is dependent on the activation energy (E_a). In experiments by Schmitt et al. (1989); Faure et al. (2015), E_a was determined to be 5370 K. This has been determined for pure water ice, while on Ganymede water ice is not pure but instead mixed with other molecules, for example CO_2 or dust (Bockelée-Morvan et al. in prep.). In Delitsky & Lane (1998), it is concluded that hydrogen-bonding effects of for example CO or CO_2 act as a counteracting force to the crystallisation process. This implies that crystallisation takes longer in a mixed substance.

Figure 8 shows the effect of increasing E_a on the model by 30%. In this case, amorphisation is the driving process at all temperatures. This is due to the fact that increasing E_a induces a lower crystallisation rate. However, amorphisation occurs much faster than what is observed on Ganymede. Therefore, the penetration depth (d) should be analysed as well. In order to match the observations, d is set to 0.15 μm. According to research of Cruz-Diaz et al. (2014) this is a reasonable value for Ly-α photons. This implies that the longitudinal decrease in CF can be caused by amorphisation due to UV irradiation.

There are also other methods to determine the crystallisation time. Research of Tonauer et al. (2023) shows how the crystallisation fraction can be calculated as a function of time and crystallisation rate at a constant temperature. The crystallisation rate of Amorphous Solid Water (ASW) is determined to be 10^{-3} or 10^{-2} depending on the film thickness according to Maté et al. (2012) and Harada et al. (2020) respectively. This is the same order of magnitude as the previous described model, making its usage valid.

To summarise, longitudinal variations in crystallinity could be caused by the amorphisation process due to UV irradiation being faster than the crystallisation process. Even though laboratory research has shown that ice does not amorphise at Ganymede's

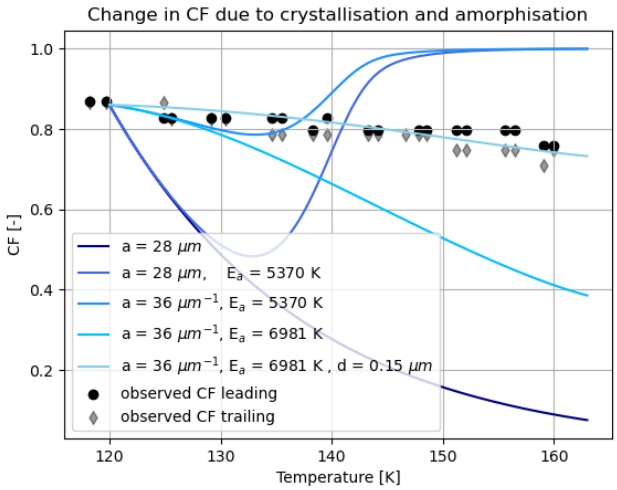

Fig. 8. Change in CF due to amorphisation (a = 28 μm), crystallisation (a = 28 μm, E_a = 5370 K) and changing the absorption coefficient, activation energy and penetration depth. Note that the penetration depth only changes from 0.1 to 0.15 μm where indicated. The dots and diamonds represent the observed CF at low latitudes at the leading and trailing hemisphere respectively.

surface temperature, the observations show that crystalline ice becomes more amorphous due to UV photons during a day on Ganymede. This could be explained by a lower crystallisation rate due to impurities in water ice. Furthermore, impacts of high energetic particles from the Jovian Plasma Sheet (JPS) can cause the ice to amorphise as well, which is not taken into account in the model. The combination of energetic impacts and UV irradiation may explain the amorphisation occurring during a day on Ganymede.

5.3. Terrains

Ganymede's surface is covered by two terrain types as well as many craters. In the crystallinity maps of figure 5, one of these craters is visible at the top right of the leading hemisphere having a slightly different crystallinity and Fresnel peak position than its surrounding area. This crater is the 92 km diameter Tros crater (Ravine et al. 2022). The crater seems to contain more amorphous ice than its surroundings. A reason for this could be a temperature difference due to the higher albedo of the crater. This could delay the crystallisation process, resulting in more amorphous ice.

6. Conclusions

This paper has shown the distribution of the crystallinity of water ice over the surface of Ganymede, using JWST NIRSpec IFU observations of the satellite's leading and trailing hemisphere. The position of the Fresnel peak at 3.1 μm is used as an indicator of the crystallinity of water ice. In the maps showing the distribution of the CF over the surface of Ganymede's leading and trailing hemisphere, both latitudinal (mostly on the leading hemisphere) and longitudinal (both leading and trailing hemispheres) variations are observed.

Latitudinal variations in the crystallinity of water ice are primarily caused by impacts of energetic particles. The closed field lines of Ganymede's magnetic field shield the equatorial region of Ganymede from low energetic particles and guides them towards the poles. Therefore, signatures of amorphous ice are present at the poles of the leading hemisphere. The trailing hemisphere does not show latitudinal variations in crystallinity, highlighting that weathering is different on the two hemispheres of Ganymede.

Next to latitudinal variations, longitudinal variations are observed on both leading and trailing hemispheres. The observations show that the CF decreases during a day on Ganymede. Due to high surface temperatures on Ganymede, the expected crystallisation time is extremely short. However, UV irradiation could amorphise the ice if this process is faster than the crystallisation process. A simple kinetic model balancing crystallisation and amorphisation could explain amorphisation due to UV irradiation if crystallisation is less efficient than observed in laboratory experiments.

References

Anderson, J. et al. 1996, Nature, 384
Baragiola, R. et al. 2005, Radiation Physics and Chemistry, 72
Berdis, J., Murphy, J., & Chanover, N. 2022, The Planetary Science Journal, 3
Brown, S. et al. 2023, Journal of Geophysical Research: Planets
Clark, L. 2000, A Teacher's Guide to the Universe, 38
Cooper, J. F., Johnson, R. E., Mauk, B. H., Garrett, H. B., & Gehrels, N. 2001, Icarus, 149, 133
Cruz-Diaz, G., Caro, G., Chen, Y., & Yih, T. 2014, Astronomy and Astrophysics, 562
De Kleer, K. et al. 2021, The Planetary Science Journal
Delitsky, M. & Lane, A. 1998, Journal of Geophysical Research, 103
Famá, M. et al. 2009, Icarus, 207
Faure, M., Quirico, E., Faure, A., et al. 2015, Icarus, 261, 14
Hansen, G. 2002, Lunar and Planetary Science XXXIII
Hansen, G. & McCord, T. 2004, Journal of Geophysical Research, 109
Harada, K., Sugimoto, T., Kato, F., Watanabe, K., & Matsumoto, Y. 2020, Physical Chemistry Chemical Physics, 22, 1963
Hibbitts, C. A., Pappalardo, R. T., Hansen, G. B., & McCord, T. B. 2003, Journal of Geophysical Research: Planets, 108
Johnson, R. et al. 2004, Radiation Effects on the Surfaces of the Galilean Satellites (Cambridge planetary science)
Kay, J. & Head, J. 1999, Lunar and Planetary Science
Kivelson, M., Khurana, K., & Volwerk, M. 2002, Icarus, 157
Kivelson, M. et al. 1996, Nature, 384
Klinger, J. 1985, JOURNAL DE PHYSIQUE
Kouchi, A., Kimura, Y., Kitajima, K., et al. 2021, Frontiers in Chemistry, 9
Kouchi, A. & Kuroda, T. 1990, Letters to Nature, 344
Kouchi, A. & Kuroda, T. 1991
Leblanc, F. et al. 2017, Icarus, 293
Leto, G. & Baratta, G. A. 2003, Astronomy and Astrophysics, 397
Ligier, N. et al. 2019, Icarus, 333
Mastrapa, R. et al. 2009, The Astrophysical Journal, 701
Maté, B., Rodríguez-Lazcano, Y., & Herrero, V. 2012, Physical Chemistry Chemical Physics, 30
McCord, T. et al. 1997, SCIENCE, 278
Mitchell, E. et al. 2017, Icarus, 285
Mura, A. et al. 2020, Journal of Geophysical Research: Planets
Pappalardo, R. et al. 2004, Geology of Ganymede (Cambridge University Press)
Paranicas, C. et al. 2018, Icarus, 302
Patterson, G. et al. 2009, Icarus, 207
Plainaki, C. et al. 2022, The Astrophysical Journal, 940
Poppe, A., Fatemi, S., & Khurana, K. 2018, Journal of Geophysical Research: Space Physics, 123
Prockter, L., Figueredo, P., et al. 2000, Journal of Geophysical Research, 105
Ravine, M. et al. 2022, Geophysical Research Letters, 49
Roth, L., Ivchenko, N., Gladstone, G., et al. 2021, Nature Astronomy, 5
Schmitt, B., Espinasse, S., Grim, R., Greenberg, J., & Klinger, J. 1989, Physics and Mechanics of Cometary Materials, 302, 65
Schmitt, B. et al. 1998, Solar System Ices
Stephan, K., Hibbitts, C., & Jaumann, R. 2020, Icarus, 337
Stephan, K. et al. 2021, Minerals, 1328
Tachibana, S. et al. 2017, SCIENCE ADVANCES, 3
Tonauer, C., Fidler, L., Giebelmann, J., et al. 2023, The Journal of Chemical Physics, 158
Trumbo, S. K., Brown, M. E., Bockelée-Morvan, D., de Pater, I., & Fouchet, T. 2023, Sciences Advances
Vance, S. et al. 2014, Planetary and Space Science, 96
Vašíček, A. & Watney-Kaczér, H. 1960, Optics of Thin Films, Series in physics (North-Holland), 288–294
Warren, S. 1984, Applied Optics, 23

Appendix A: Crystallinity model

In order to determine whether water ice crystallises or amorphises at a certain temperature, the crystallisation and amorphisation process have to be evaluated to determine which process is dominant. For the crystallisation process, the rate is determined as described in Schmitt et al. (1989); Faure et al. (2015). The crystallisation time (equal to 1/rate) is defined as shown in equation A.1, where A is the pre-exponential factor equal to $9.54 \cdot 10^{-14}$ s, E_a is the activation energy equal to 5370 K and T is the temperature in Kelvin.

$$t_{crys} = A \cdot e^{-E_a/T} \tag{A.1}$$

In order to calculate the amorphisation time, the dose (D) of photons that will be absorbed has to be calculated first which can be done using to equation A.2 (Leto & Baratta 2003). Here F is the flux that is able to amorphise water ice ($\lambda < 207$ nm) equal to $7.6 \cdot 10^{11}\ eV \cdot cm^{-2} \cdot s{-}1$ on Ganymede (Cooper et al. 2001), a is the absorption coefficient in μm^{-1}, d the penetration depth that is assumed to be 0.1 μm for UV photons (Kouchi et al. 2021) and n the number of molecules per cm^2 equal to 10^{15} (Clark 2000). When the irradiation dose is known, the amorphisation time can be determined using equation A.3. Here r_{am} is the amorphisation rate in s^{-1} and k is the cross-section equal to 0.68 molecules per eV for Ly-α photons (Leto & Baratta 2003).

$$D = \frac{F \cdot e^{-a \cdot d}}{n} \tag{A.2}$$

$$t_{am} = \frac{1}{r_{am}} = D \cdot k \tag{A.3}$$

Figure A.1 shows the resulting model for amorphisation and crystallisation. It can be seen that amorphisation dominates at low temperatures and crystallisation starts dominating above approximately 130K. From the figure it can be seen that the amorphisation time is not constant as would be expected since it does not depend on temperature in the shown equations. However, in reality the flux will not be equal over the surface of Ganymede due to its curvature. Therefore, a simple function relating the angle at which the flux hits the surface of Ganymede and the surface temperature is implemented. It is known that the temperature is 160 K at a 0 incidence angle and it is assumed that the temperature is 120 K at 60. Using these two points a linear function is composed, relating temperature and angle. The flux is then multiplied by $\cos(\theta)$, meaning that there is less flux at lower temperatures.

In order to assess how crystallinity changes during a day on Ganymede, a simple model was made, as shown in equation A.4. Here, N_i and N_{i-1} are the crystallinity fraction at the current and previous time step respectively, r_{am} and r_{crys} are the amorphisation and crystallisation rate and Δt is the time step.

$$N_i = N_{i-1} - r_{am} \cdot \Delta t \cdot N_{i-1} + r_{crys} \cdot \Delta t \cdot (1 - N_{i-1}) \tag{A.4}$$

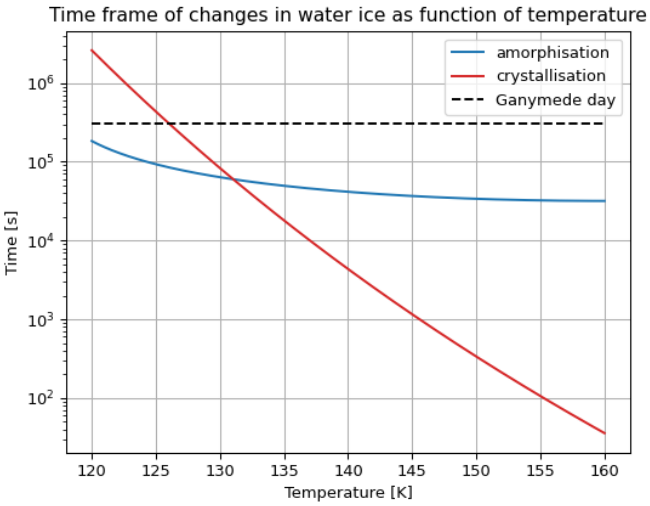

Fig. A.1. Crystallinity model showing the crystallisation and amorphisation time. In the amorphisation model, an absorption coefficient of 28 μm^{-1} is used, similar to lab experiments by Leto & Baratta (2003). A day on Ganymede is indicated showing that most processes can occur on a daily basis on the moon.

To relate the crystallinity fraction to temperature, it was assumed that it takes about 40h, which is half of the daytime on Ganymede, to warm up Ganymede's surface by 40K from morning to midday. Including the rate of 1K/h to the model results in the plot shown in figure A.2. In the figure it can be seen that amorphisation dominates at low temperatures and after approximately 130K crystallisation is beginning to take over. This is in line with figure A.1.

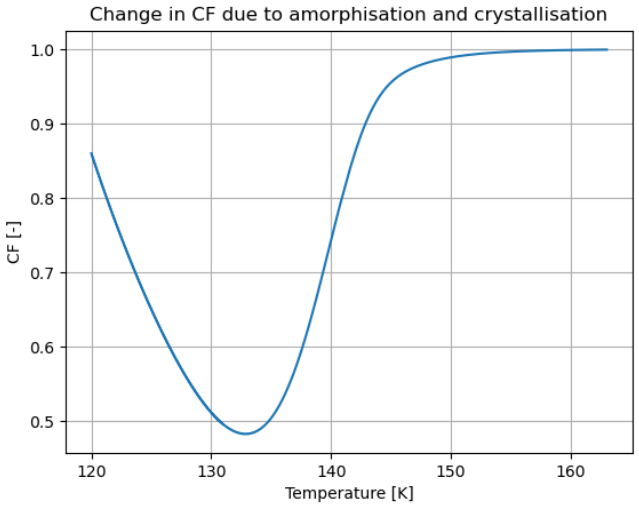

Fig. A.2. Model that shows the change in CF due to amorphisation and crystallisation.

In the previous calculations, a constant absorption coefficient was used to calculate the amorphisation rate based on lab experiments (Leto & Baratta 2003). However, the absorption coefficient is a function of wavelength. It can be calculated as shown in equation A.5, where k is the imaginary part of the refraction index.

$$a = \frac{4\pi k}{\lambda} \tag{A.5}$$

The optical constants at UV wavelengths determined by Warren (1984) used for this model. Figure A.3 shows how the amorphisation time changes for different absorption coefficients. This is done for the minimum, maximum and mean absorption coefficient at UV wavelengths. Since the absorption coefficient is a measure of how far photons can penetrate through a medium before they are absorbed, amorphisation time increases with increasing absorption coefficient.

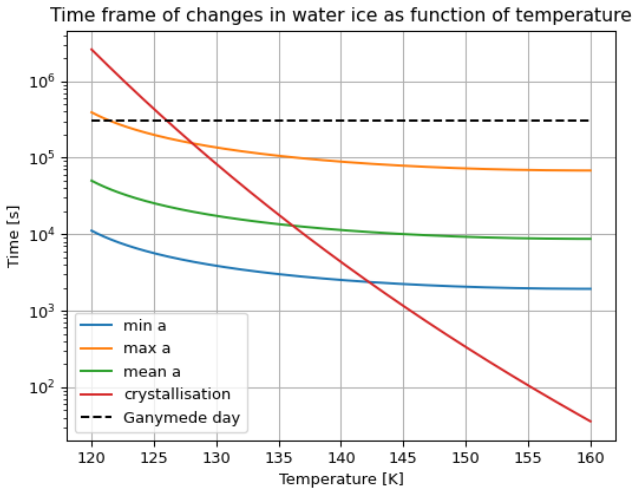

Fig. A.3. Effect of varying absorption coefficient on the amorphisation time.

3

Conclusions and recommendations

This chapter closes the research into the JWST observations of Ganymede. First conclusions of the research are drawn by answering the established research questions in section 3.1. Next recommendations will be for future work are discussed in section 3.2.

3.1. Conclusions

This section answers the established research questions, using the work presented in the journal article and the additional results in appendix B.

1. **How can variations in crystallinity of water ice be linked to energetic processes occurring on the surface of Ganymede?**

   The crystallinity of water ice on the surface of Ganymede is investigated with JWST NIRSpec IFU observations of the satellite's leading and trailing hemisphere. The position of the Fresnel peak at 3.1 μm is used as an indicator of the crystallinity of water ice. In the maps showing the distribution of the CF over the surface of Ganymede's leading and trailing hemisphere, both latitudinal (mostly on the leading hemisphere) and longitudinal (both leading and trailing hemispheres) variations are observed.

   Latitudinal variations in the crystallinity of water ice are primarily caused by impacts of energetic particles. The closed field lines of Ganymede's magnetic field shield the equatorial region of Ganymede from low energetic particles and guides them towards the poles. Therefore, signatures of amorphous ice are present at the poles of the leading hemisphere. The trailing hemisphere does not show latitudinal variations in crystallinity, highlighting that weathering is different on the two hemispheres of Ganymede.

   Next to latitudinal variations, longitudinal variations are observed on both leading and trailing hemispheres. The observations show that the CF decreases during a day on Ganymede. Due to high surface temperatures on Ganymede, the expected crystallisation time is extremely short. However, UV irradiation could amorphise the ice if this process is faster than the crystallisation process. A simple kinetic model balancing crystallisation and amorphisation could explain amorphisation due to UV irradiation if crystallisation is less efficient than observed in laboratory experiments.

2. **What can NIRSPec high resolving power observations reveal about CO_2 abundance in Ganymede's exosphere?**

   One of the primary objectives of the ERS program of Ganymede observations was to detect exospheric CO_2 gas. In order to do so, NIRSpec's dispersion-filter combination with the highest possible resolving power in the desired wavelength range was used for the observations. Nonetheless, gaseous CO_2 was not detected in leading nor in trailing hemisphere observations.

This implies that CO_2 does not have a high abundance in Ganymede's exosphere.

3. **What can the CO_2 $\nu 3$ absorption band reveal about the state and distribution of CO_2 on Ganymede's surface?**

   When mapping the CO_2 $\nu 3$ band, two parameters were taken into consideration. The band depth is a measure of the abundance of CO_2 and the band position gives insight into the mixture of CO_2. From the band depth it was deduced that for both leading and trailing hemisphere's CO_2 is more abundant at low latitudes. A correlation between the CO_2 abundance and bond albedo was not found at the leading hemisphere. On the trailing hemisphere the band depth seems anti-correlated with albedo.

   The band centre at the poles of both hemispheres is close to pure CO_2, implying that pure CO_2 is trapped in water ice in this region. At lower latitudes a blueshift is seen. This implies that CO_2 is mixed in this region. Since water ice the most abundant molecule on Ganymede's surface, it makes sense that CO_2 could be mixed with water ice. However, lab experiments do not seem to find the proper ratio between CO_2 and water molecules to explain the observed band. Next to water, CO_2 could also be mixed with non-ice components for example cometary dust consisting of organic matter.

4. **Can NIRSpec's high resolving power observations gain more insight into the distribution of organic material on the surface of Ganymede?**

   A second reason to do observations with the highest possible resolving power is to allow the detection of faint features. For example, the H_2O_2 signature was found at the poles of the leading hemisphere. Furthermore, an absorption band was detected at 3.42 μm which is the expected wavelength of the asymmetric stretching mode of CH_2. The detection of this band was no big surprise as the NIMS and the JIRAM instrument detected the band as well. However, the JWST is capable of mapping the feature over the surface of Ganymede due to its distance to the moon. Nonetheless, maps of the band area do not result in a clear distribution. The features can not be linked to terrain and latitudinal variations are not visible either. In addition, other stretching modes are not detected making it hard to gain information about the formation, abundance or distribution of organic material on Ganymede.

3.2. Recommendations for future research

In this section, several ideas for future research concerning the crystallinity of ice on Ganymede, the state of CO_2 and organic material are presented.

- In this research, the Fresnel factor is used as an ice model. This model assumes a normal incidence angle of light in calculating the reflectivity. In reality this might not always be the case. When using a Hapke model for example, conditions of the ice on Ganymede can be modelled and this could be used as a baseline.

- When determining the Fresnel factor, the optical constants at a constant temperature are used. However, the temperature is not the same at each observed pixel of Ganymede. By making a temperature model that provides the temperature for each pixel, the crystallinity factor can be calculated more precise at each location.

- Experiments concerning CO_2 trapped in different mixtures and with multiple ratios could be performed to investigate how the blueshifted CO_2 band on Ganymede (and other icy moons) can be explained. When this is better understood, knowledge about the origin and evolution of CO_2 on icy moons can be gained.

- In order to explain the observed decrease in CF during a day on Ganymede, certain values were chosen for the absorption coefficient, activation energy and penetration depth for the model to match the observations. Even though the values seem reasonable, it might not be the only setting that works for the observed trend. Therefore, a model could be made to see the range of values

that the three parameters can have to match the observations and which settings would make the most sense.

- Experiments can be performed investigating how water ice crystallises in a CO_2 mixture and what the effects are on the crystallisation time compared to pure water ice. This way the change in activation energy can be established more accurately, which gives a better view of the crystallisation rate.

- In order to get an even better view of the entire surface Ganymede, a cycle two observation could be done with the JWST, observing the Jovian and anti-Jovian hemisphere. This way terrain near the limb could be investigated with less noise in the spectra. Furthermore, findings of the first cycle could be extrapolated to these two sides of Ganymede's surface, where interactions with the Jovian plasma sheet might be different.

- Not much is known about the distribution of organic material on Ganymede and high resolving power observations of the NIRSpec could not provide more insight than the detection of the 3.42 band. Future missions might be able to gain more insight into organic material. The JUpiter Icy Moons Explorer's (JUICE) main target is Ganymede and it will be the first probe to orbit the satellite. Due to the low spatial resolution of its Moons and Jupiter Imaging Spectrometer (MAJIS), it might be possible to get a better view of the distribution of organic material and linking it to different terrain types. However, JUICE will not arrive at the Jovian system for almost a decade meaning that it will take some time before data is available.

A

Data acquisition

Before absorption features in reflectance spectra can be analysed, the data has to be retrieved and calibrated. At the start of this research in August 2022, the JWST pipeline was not yet capable of calibrating the spectra. Therefore, during the first months of the thesis a lot of time was dedicated towards the calibration and optimisation of the spectra, which will be discussed in this chapter. First, the data retrieval will be explained in section A.1. Then the Doppler shift corrections needed to filter out the Solar lines are discussed in section A.2 and finally the pipeline calibration process will be discussed in section A.3.

A.1. Data retrieval

The JWST data is open source and can be accessed using the Mikulski Archive for Space Telescopes (MAST) platform [1]. Using the proposal ID 1373, all the observations of the Jovian system can be found, including NIRSpec and MIRI observations. The desired data can then be downloaded in so called Flexible Image Transport System (FITS) files which is a common format in astronomy. From the name of the FITS file, the observation that is stored in the file can be derived. For example, jw01373019001_03101_00001_nrs1_uncal.fits is a JWST observation of proposal 1373. It has observations number 19, meaning it is a Ganymede leading hemisphere observation. This file is dither 1 of the four different dithers and the detector is nrs1. Furthermore, this example is an uncalibrated file meaning that the data is not yet processed with the pipeline.

The data can be downloaded from the MAST at any stage in the pipeline. Uncalibrated files are accessible and required to use if the pipeline does not function as desired. However, calibrated files can also be downloaded. At the start of the thesis, level 2 data was used meaning that the first two steps of the pipeline were run.

Once the proper FITS files are downloaded, they can be imported into a python environment. For this thesis, Jupyter notebooks were used. In order to access the data, one must understand how the data is stored. Every FITS file contains data cubes. For each observed wavelength, the flux values for all NIRSpec's IFU pixels are known. In order to generate a spectrum, the average flux at each wavelength is determined over the disk of Ganymede. In this process, bad pixels are filtered out. Using the z-score, the standard deviation of all flux values at a certain wavelength can be determined. This way the outliers (standard deviation higher than 4) will not be taken into consideration. An example of a resulting flux spectrum of the trailing hemisphere is shown in figure A.1. The figure clearly illustrates the presence of Solar lines which will be filtered out in order to be able to assess Ganymede's features. In order to do so, a Doppler shift has to be taken into account which will be explained in the next section.

[1] https://mast.stsci.edu/portal/Mashup/Clients/Mast/Portal.html

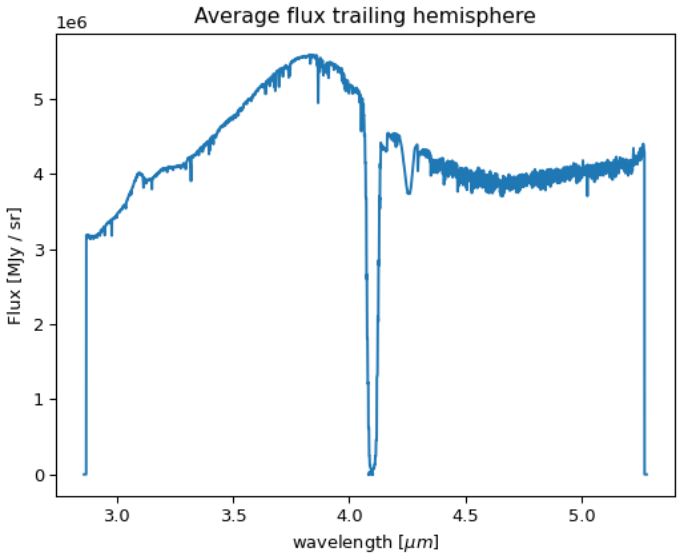

Figure A.1: Example of a flux spectrum of the trailing hemisphere of Ganymede. Note the presence of Solar lines in the spectrum.

A.2. Doppler shift

When the received flux of Ganymede is known, it is essential to properly filter out the Solar lines to be able to fully assess Ganymede's features. This is done using the Solar spectrum of R.L. Kurucz [2], which can be seen in figure A.2 for the wavelength range of the NIRSpec observations.

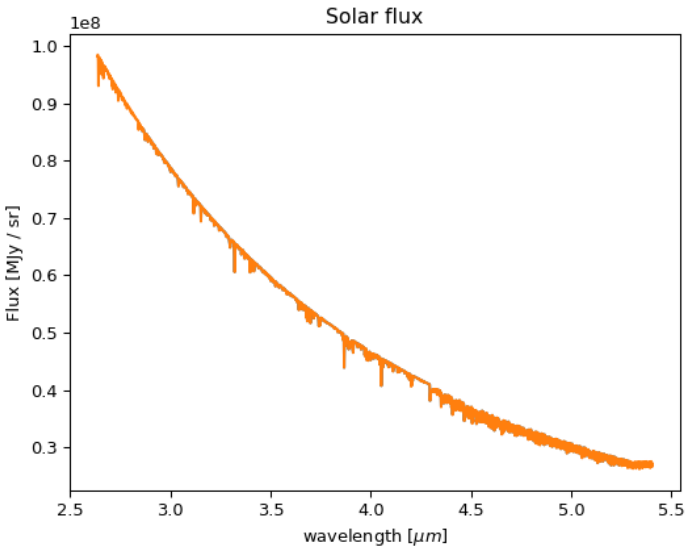

Figure A.2: Solar spectrum of R.L. Kurucz at the relevant wavelengths of the NIRSpec observations

Before dividing the received flux by the Solar spectrum, a Doppler shift has to be taken into account as the available Solar spectrum is in a Solar inertial reference frame. Light leaves the Sun, is reflected on Ganymede and then detected by the JWST. Therefore, two shifts have to be taken into account when filtering the Solar lines. One shift accounting for the heliocentric shift of Ganymede and one shift accounting for Ganymede's velocity with respect to the JWST. The Doppler shift ($\Delta\lambda$) can then be calculated using equation A.1, where λ_{obs} is the observed wavelength, λ is the wavelength, V is the velocity that causes the Doppler shift and c is the speed of light.

[2] http://kurucz.harvard.edu/sun.html

$$\frac{\Delta\lambda}{\lambda} = \frac{\lambda_{obs} - \lambda}{\lambda} = \frac{V}{c} \tag{A.1}$$

Since Ganymede is the target of the observations, both Doppler shifts should be expressed in a Ganymede reference frame. For the Doppler shift caused by Ganymede moving with respect to the JWST, this is done using equation A.2. For the shift caused by Ganymede moving with respect to the Sun, this is done using equation A.3. The velocity of the JWST with respect to Ganymede ($V_{G/JWST}$) and the velocity of Ganymede with respect to the Sun ($V_{S/G}$) are taken from the horizon database of the Jet Propulsion Laboratory [3]. In the database, the radial velocities required can be found at the time of the observations. During the observation time, the radial velocity does not change significantly so the velocity at the start of the observation is used. The velocity of Ganymede with respect to the Sun is found to be -10.8 km/s and 10.6 km/s for the leading and trailing hemisphere respectively. The velocity of Ganymede with respect to the JWST is found to be -31.9 km/s and -11.6 km/s respectively.

$$\lambda_{Gan} = \frac{\lambda_{JWST}}{\frac{V_{G/JWST}}{c} + 1} \tag{A.2}$$

$$\lambda_{Gan} = \lambda_{Sun} \cdot \left(\frac{V_{S/G}}{c} + 1\right) \tag{A.3}$$

After applying the Doppler shift and converting to the radiance factor (I/F), Solar lines would still remain visible in the spectra. Therefore, an additional shift is applied to optimally remove the Solar lines. By comparing Solar lines at 3.867 and 4.295 μm, for nrs1 and nrs2 respectively, in the Ganymede spectrum with the Solar spectrum, additional shifts of 0.168 and 0.137 nm were determined to remove the Solar lines from the spectra. These values are smaller than the resolution of NIRSpec, which is 0.665 nm.

A.3. Pipeline calibration

At the start of this research, the 1.8 pipeline version was available. This pipeline was not yet able to fully calibrate NIRSpec IFU moving target observations. Furthermore, the third pipeline stage could not be used yet as combining the four dithers resulted in noisy spectra. Figure A.3 shows a spectrum dither 1 of the leading hemisphere. In this spectrum it can be seen that some regions contain more noise than others. For example, on top of the Fresnel peak some spikes appear. Furthermore, the units on the y-axis are not correct as they are orders of magnitudes lower than they should be.

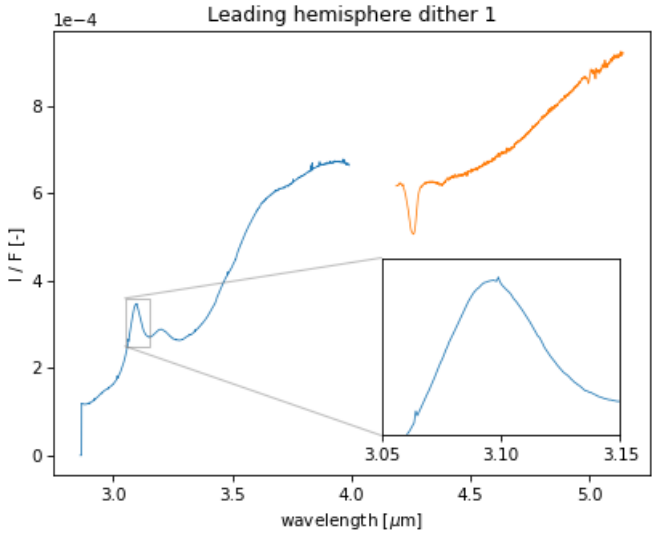

Figure A.3: Spectrum of dither 1 of the leading hemisphere. In the inset, spikes in the Fresnel peak are illustrated.

[3] https://ssd.jpl.nasa.gov/horizons/app.html#/

Figure A.4 shows two dithers of trailing hemisphere level 2 data. In the spectra even more noise can be seen. Furthermore, there is a difference of a few orders of magnitude for the I/F values for the two dithers. Again spikes are observed in the Fresnel peak as illustrated in the spectrum of dither 1. The shape of the Fresnel peak of dither 4 looks very strange as can be seen in the figure, making the calibration slightly unreliable. The combination of the many spikes in the spectra and the unusual shape of the Fresnel peak made it challenging to extract and map features from the observations.

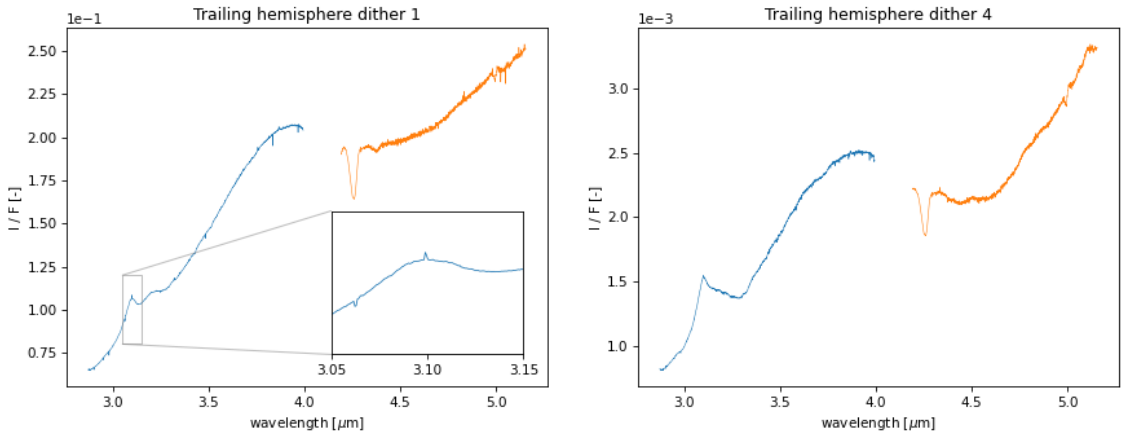

Figure A.4: Spectra of dithers 1 and 4 of the trailing hemisphere.

In December 2022, the JWST pipeline was updated to its current version 1.9. In this update, the problems with the NIRSpec IFU moving target observations were fixed. This meant that level 3 data with all dithers combined could be used. However, the pipeline has to be run locally for the best results. The jwst python package is not compatible for Windows so it had to be run using Linux on the Eudoxos server. Using Filezilla, the FITS files could then be transferred to a local device. The updated level 3 spectra will be presented and discussed in appendix B.

B

Additional Results

The Journal Article presented in chapter 2 is the main focus of this thesis. However, during the thesis other results were obtained and are discussed in this chapter. First the spectra obtained by the NIRSpec observations will be shown in section B.1. Several features will be discussed, starting with water ice in section B.2. Then CO_2 will be discussed in section B.3 and finally the presence of organics will be debated in section B.4.

B.1. NIRSpec observations

In August 2022, the NIRSpec IFU observed the leading and trailing hemisphere of Ganymede. Solar lines are removed using a Solar spectrum of R.L. Kurucz [1] and matched with the observations by applying a Doppler shift as explained in section A.2. The obtained spectra are shown in figure B.1. In the spectra, the 4 - 4.15 μm range is excluded. This is because the signal is detected by two detectors in the NIRSpec instrument, nrs1 and nrs2. Inbetween these two detectors, there is a physical gap which excludes the 4 - 4.15 μm range from the spectra. This gap unfortunately prevents the detection of SO_2 at 4.05 μm.

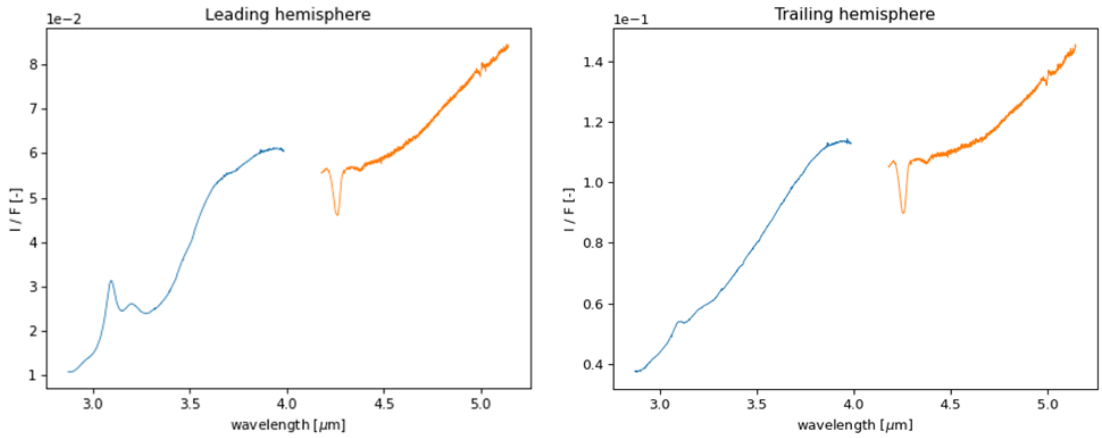

Figure B.1: Reflectance spectra of Ganymede's leading (observation 19) and trailing (observation 28) hemisphere obtained by NIRSpec's IFU.

For both hemispheres, the two features that immediately struck the eye are the Fresnel peak of water ice at 3.1 μm and the CO_2 band at 4.26 μm. Furthermore, signatures of H_2O_2 can be found on the leading hemisphere at 3.5 μm as confirmed by Trumbo et al. (2023). This feature is less visible on the trailing hemisphere as its presence is correlated with the abundance of water ice, which is also lower on the trailing side of Ganymede.

[1] http://kurucz.harvard.edu/sun.html

B.2. Water ice

Water ice is the most abundant molecule on the surface of Ganymede and therefore dominates its reflectance spectra (McCord et al., 1998). Figure B.2 shows maps of the abundance of water ice over the surface of Ganymede using the Fresnel peak and the water ice interband. The first maps show the equivalent width of the Fresnel peak, which is equal to the area of the peak. It can be calculated as shown in equation B.1 (Stahler and Palla, 2005), where F_c is the flux of the continuum underneath the peak and F_s is the flux of the spectrum.

$$W_\lambda = \int \frac{F_c - F_s}{F_c} d\lambda \tag{B.1}$$

From the area of the Fresnel peak, it becomes visible that most water ice is concentrated on the poles of the leading hemisphere of Ganymede. Around the equator there is some water ice depending on the terrain. It can be seen on the map that the dark terrains contain much less water ice than the bright terrains, which is in accordance to earlier research (Patterson et al., 2009). Furthermore, the 92 km diameter Tros crater can be seen on the top right on the leading hemisphere, containing more water than its surroundings (Ravine et al., 2022).

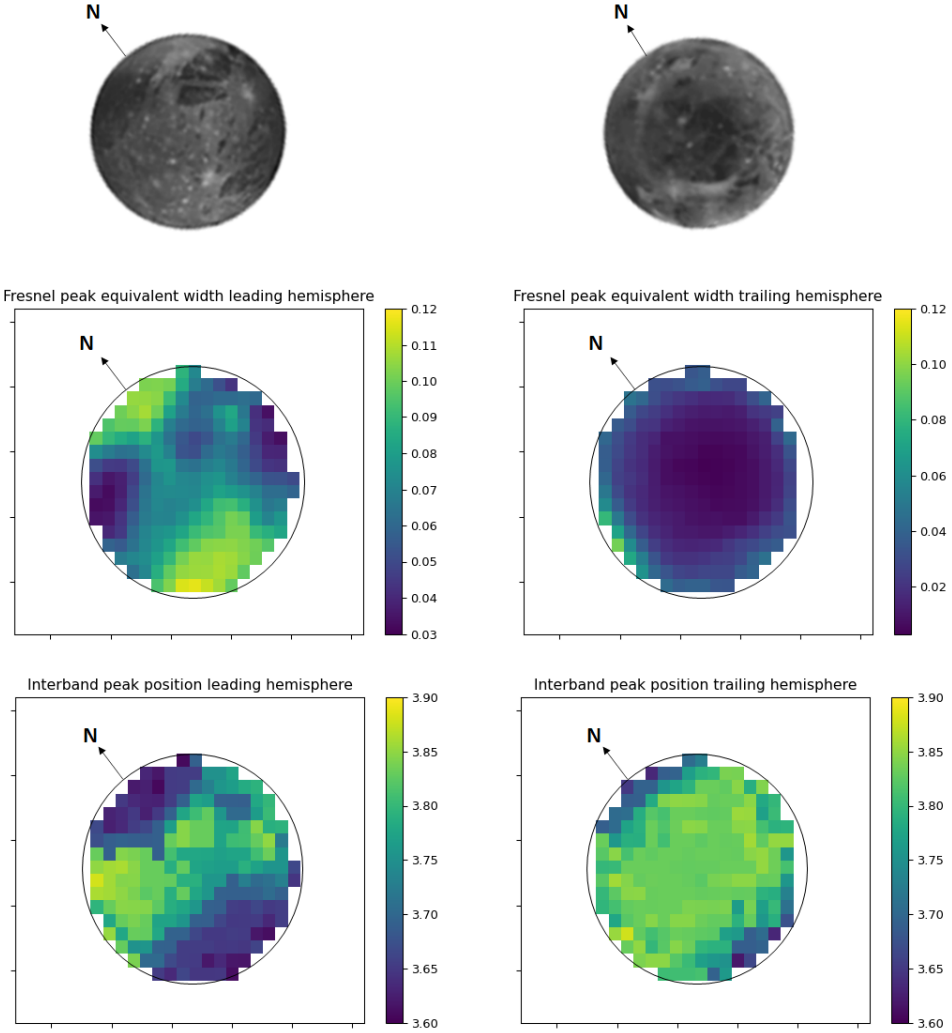

Figure B.2: Maps of the equivalent width of the Fresnel peak for the leading (left) and trailing (right) hemisphere. The bottom maps show the interband peak position. In the maps, the North is pointing towards the top left as indicated by the arrow.

The maps at the bottom of figure B.2 show the peak position of the water ice interband. Spectra of water ice contain two large bands centred at around 3 and 4.4 μm approximately as shown on the left in figure B.2. In between these bands is the so called interband located at 3.6 μm. Figure B.3 shows how this interband changes with temperature. It can be seen that the peak value of the interband shifts to higher wavelengths with increasing temperature. In the figure, the blue line indicates the interband position according to a Hapke model by Mastrapa et al. (2009). It can be seen that the band is shifted to lower wavelengths in this model, which does not agree with laboratory experiments. This is due to an error in the optical constants in the 3.2 - 5 μm range (Clark et al., 2012).

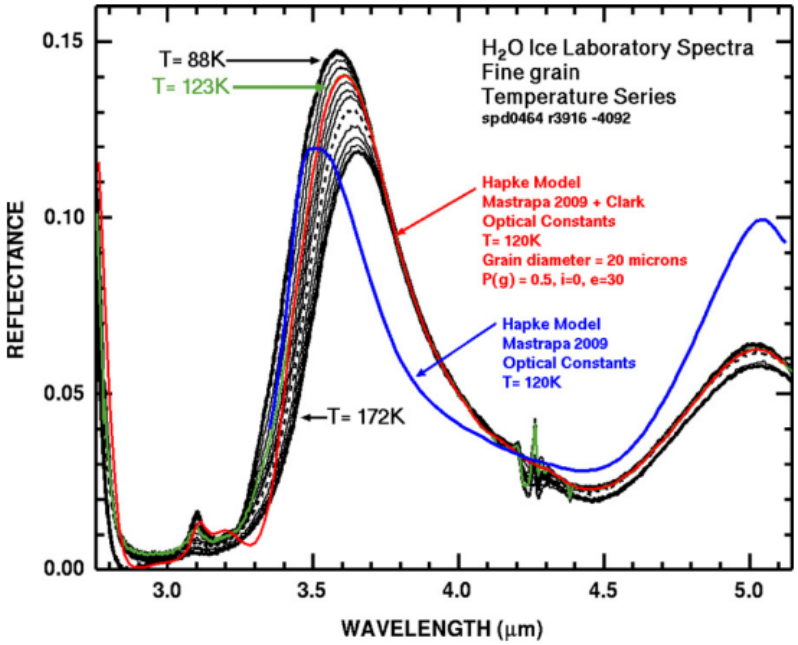

Figure B.3: Reflectance spectra of crystalline water ice, showing the 3.6 μm interband (Clark et al., 2012). The interband position shifts to higher wavelengths at higher temperatures.

Research of Leblanc et al. (2017) shows that the surface temperature on Ganymede is on average 110 K approximately. This means that for pure water ice one would expect the interband to peak at about 3.6 μm. From figure B.2 it can be seen that the peak value ranges from 3.6 μm at the poles to 3.9 μm at lower latitudes. This means that the water ice is mixed with other molecules when moving away from the poles since a peak of 3.9 μm is not seen in pure water ice spectra. Note again the presence of the Tros crater on the leading hemisphere, which contains more water than the surrounding terrain.

B.3. CO_2

Besides water ice, CO_2 has the highest abundance on Ganymede. The presence of CO_2 was discovered using the 4.26 μm absorption band in NIMS spectra (Hibbitts et al., 2003). This band represents the asymmetric stretching mode ($\nu 3$) of CO_2, which has its band centre at 4.27 μm (K. Isokoski and Linnartz, 2013). In figure B.4, the latitudinal variations of the band as observed on Ganymede are shown for both hemispheres. It can be seen that the band behaves different at different latitudes, especially for the leading hemisphere. On the poles of the leading hemisphere, the band centre is at a similar wavelength as pure CO_2. However, at the equator the band is blueshifted towards slightly lower wavelengths indicating that the CO_2 is mixed. For the trailing hemisphere, the latitudinal variations seem less evident. However, all the bands seem to be blueshifted when compared to pure CO_2 ice.

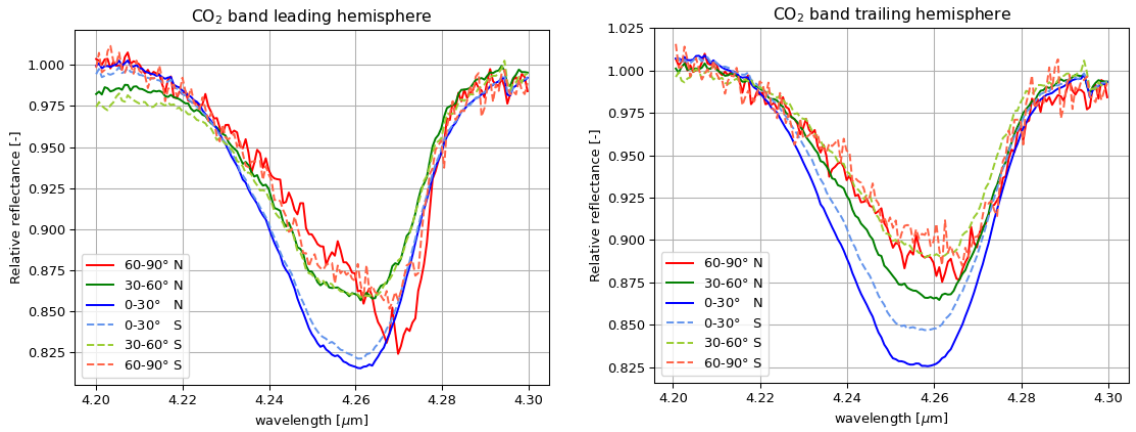

Figure B.4: CO_2 $\nu 3$ absorption band for indicated latitudinal ranges for the leading (left) and trailing (right) hemisphere.

One of the objectives of the NIRSpec observations was to detect the exospheric CO_2 $\nu 3$ band. Therefore, the highest possible resolution was used for the observations. As can be seen in figure B.5, a high resolution is required to detect the rotational and vibrational modes of a gas in a reflectance spectrum. Note that the figure is a spectrum of CO gas. However, the reasoning is similar for CO_2 and observation of CO_2 gas should show the rotational- vibrational modes of the CO_2 molecule. Besides some noise in the JWST spectra, this is not seen in figure B.4. Therefore, it can be concluded that the abundance of gaseous CO_2 in Ganymede's exosphere is low.

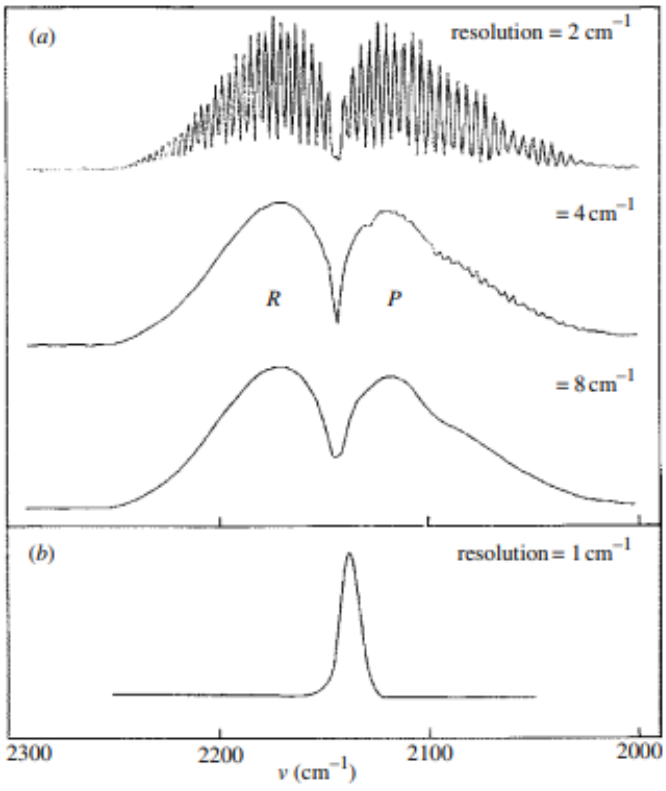

Figure B.5: Spectra of CO molecules for different spectral resolutions in the gas phase (a) and solid phase (b) (Tielens, 2005).

Figure B.6 visualises the observed changes in band position over the disk of Ganymede for the leading and trailing hemisphere. In addition, the bottom two maps show the distribution of the band depth over the surface which is an indication of the abundance of CO_2. The definition of the band depth (BD) is given in equation B.2 (Pommerol and Schmitt, 2008). Here, R(λ) is the reflectance at the wavelength

of maximum absorption and $R_c(\lambda)$ is the value of the continuum at the same wavelength. In contrary to water ice, CO_2 is mostly concentrated at the equator for both leading and trailing hemisphere.

$$BD(\lambda) = 1 - \frac{R(\lambda)}{R_c(\lambda)} \tag{B.2}$$

Hibbitts et al. (2003) stated in their research that little or no CO_2 is detected at the poles. From the band depth maps in figure B.6, it can be seen that indeed less CO_2 is present near the poles and most of the CO_2 is present around the equator. From the band centre maps it can be seen that the CO_2 present at the poles of the leading hemisphere is pure CO_2 probably trapped in a water matrix. Near the equator, the CO_2 is mixed with a substance which can be seen from the blueshifted band centre.

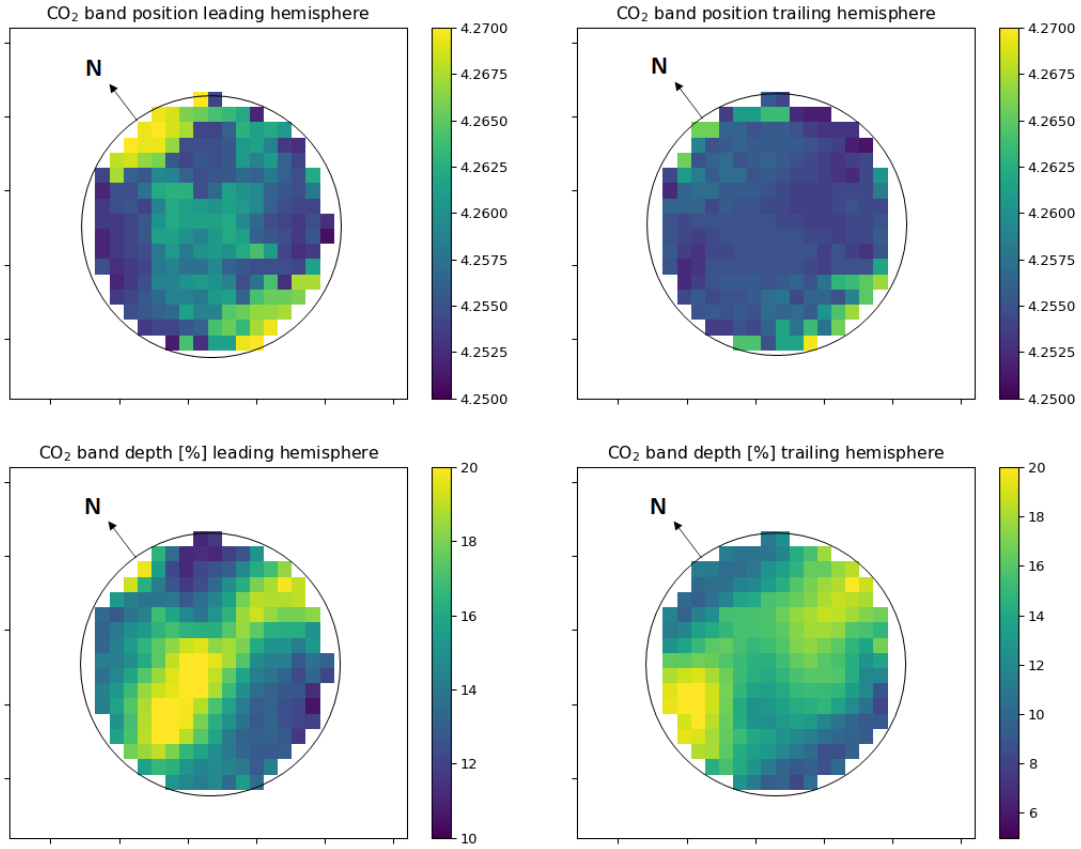

Figure B.6: Maps of the CO_2 band position (top) and band depth (bottom) for Ganymede's leading (left) and trailing (right) hemisphere.

The research of Hibbitts et al. (2003) also states that bright terrains contain less CO_2 than dark terrains. Figure B.7 shows the bond albedo of Ganymede's leading and trailing hemisphere. The lower the albedo value, the darker the terrain. Figure B.8 shows how the band depth is correlated with albedo and thus terrain. For the leading hemisphere, there is no clear correlation between the two parameters. On the trailing hemisphere it can be seen that higher albedo terrain seems to have a low CO_2 abundance, contradicting the statement of Hibbitts et al. (2003).

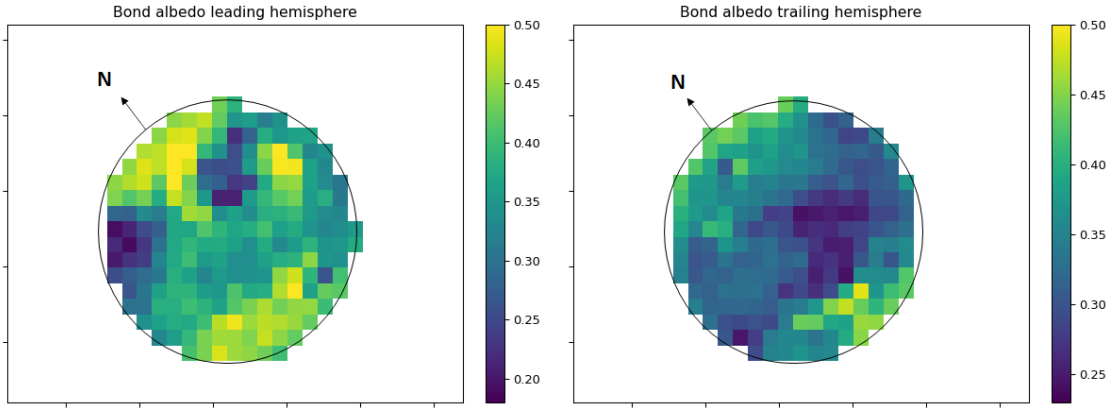

Figure B.7: Maps of the bond albedo for leading (left) and trailing (right) hemisphere, derived from (De Kleer et al., 2021) are shown. The mean albedo of the surface area of every NIRSpec IFU pixel is taken.

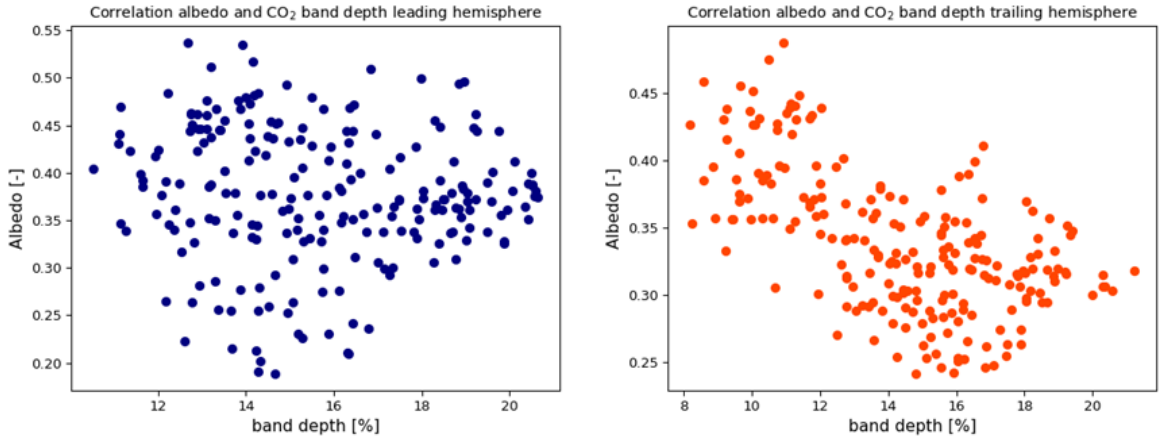

Figure B.8: Correlation between bond albedo and band depth of the CO_2 absorption band for leading (left) and trailing (right) hemisphere.

The fact that the CO_2 band centre has shifted at low latitudes for both leading and trailing hemisphere is most likely to be caused by the CO_2 being mixed. Jones et al. (2014) investigated this shift for a similar band on Callisto. It was found that carbonic acid (H_2CO_3) irradiated with electrons has a similar band as the observed CO_2 band on Callisto. However, in figure B.9, it can be seen that this is not an optimal fit for the observed CO_2 band at low latitudes on Ganymede. In the figure, a few other options of a CO_2 and H_2O mixture at different ratios and temperatures are shown to see what gives the best match with the observed shift in CO_2 band centre. However, none of these options seem to fit the observed bands properly. According to Bockelée-Morvan et al. (in prep.) the mixture is thought to be CO_2 adsorbed or trapped on non-icy materials, such as minerals or salts.

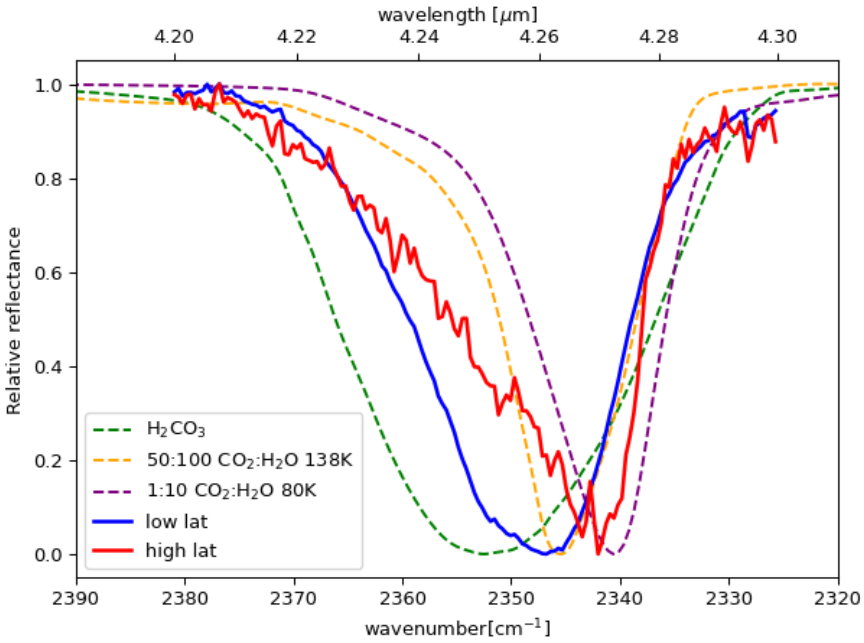

Figure B.9: Influence of mixing CO_2 on the band shape and position for several mixtures and temperatures (Ehrenfreund et al., 1999; Jones et al., 2014; He et al., 2018).

B.4. Organics

In the reflectance spectra obtained by the NIMS on board the Galileo spacecraft and the Jovian Infrared Auroral Mapper (JIRAM) on board the Juno spacecraft, organic features are detected (McCord et al., 1997; Pappalardo et al., 2004; Mura et al., 2020). However, in the analysis of the spectra of both NIMS and JIRAM it is mentioned that these features are very shallow due to low concentration of the compounds and the low instrumental signal-to-noise. Therefore, it is hard to see them right away in the spectra. To assess whether organics are detected by NIRSpec's observations, the data is fit with a fifth order polynomial. In doing so, two wavelength ranges centred around 3.42 and 3.5 μm are excluded as these are the locations of the expected organic feature and the confirmed H_2O_2 band (Trumbo et al., 2023). The continuum that is obtained is shown in figure B.10.

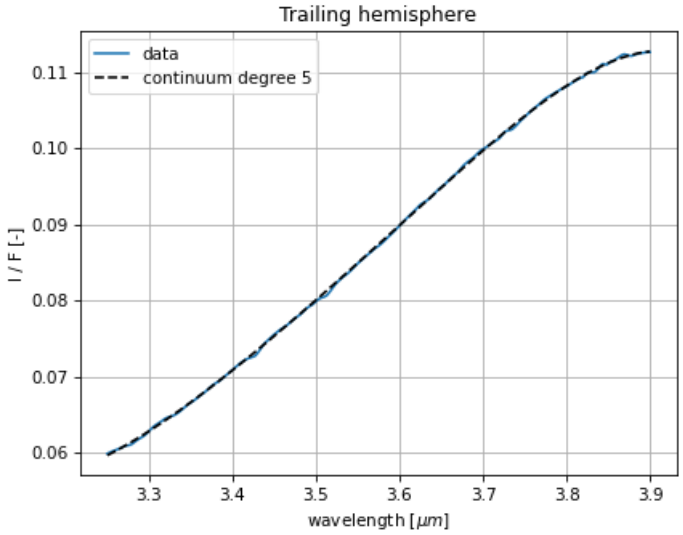

Figure B.10: Example of a continuum fit in the 3.275 - 3.9 μm region.

After estimating the true continuum, it is subtracted from the data. This way faint absorption features become better visible. The result is shown in figure B.11 for both leading and trailing hemisphere. The graphs also indicate common stretching modes of organic material and where they are expected to occur (Merouane et al., 2014). On the leading hemisphere, the broad H_2O_2 becomes evident right away. It can also be seen on the trailing hemisphere but less prominent. Close to the asymmetric stretching mode of CH_2 at 3.42 μm, a band is visible. On the leading hemisphere, the band is very small but the upward trend is certainly broken. On the trailing hemisphere, the band seems to be more dominant. Having a band depth of about 1%, the band is even deeper than the H_2O_2 band. Compared to the dotted green line, the band seems slightly redshifted.

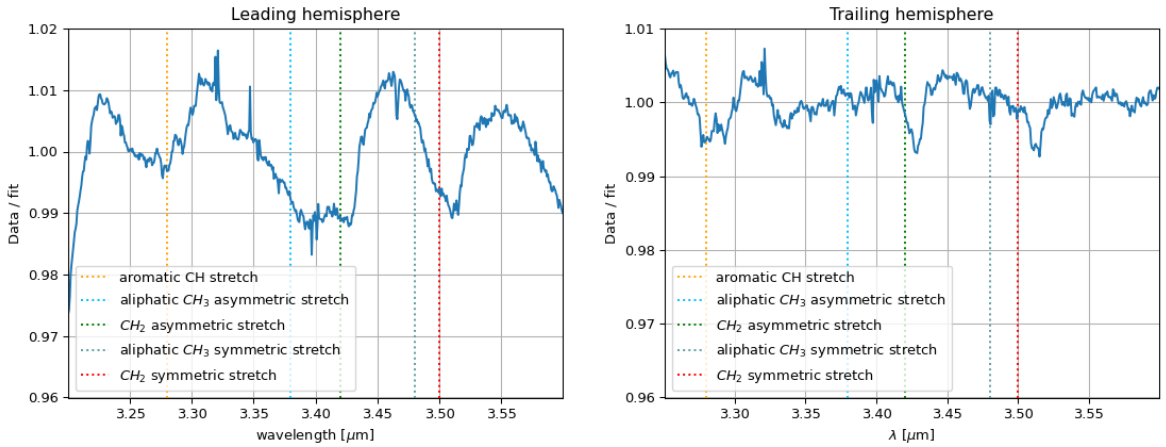

Figure B.11: Continuum subtracted spectrum for the leading (left) and trailing (right) hemisphere. The dotted lines indicate where organic stretching modes are expected to occur (Merouane et al., 2014).

Even though the observed bands are fairly small, they are larger than the noise level at low latitudes. Furthermore, the fact that the 3.42 band is observed with NIMS and JIRAM proves that this is not just instrumental noise. To further investigate the feature and its distribution over the surface of Ganymede, figure B.12 shows continuum subtracted data for several latitude ranges. For the highest latitudes, it can be seen that the noise levels are higher and more significant than for lower latitudes. This is due to the fact that the spectra contain less pixels at high latitudes and the available pixels are mostly located at the edge of Ganymede's disk thus having a lower signal-to-noise. Even though the highest latitudes are too noisy to show the band, the medium to low latitudes of both hemispheres do show signatures of a 3.42 absorption band.

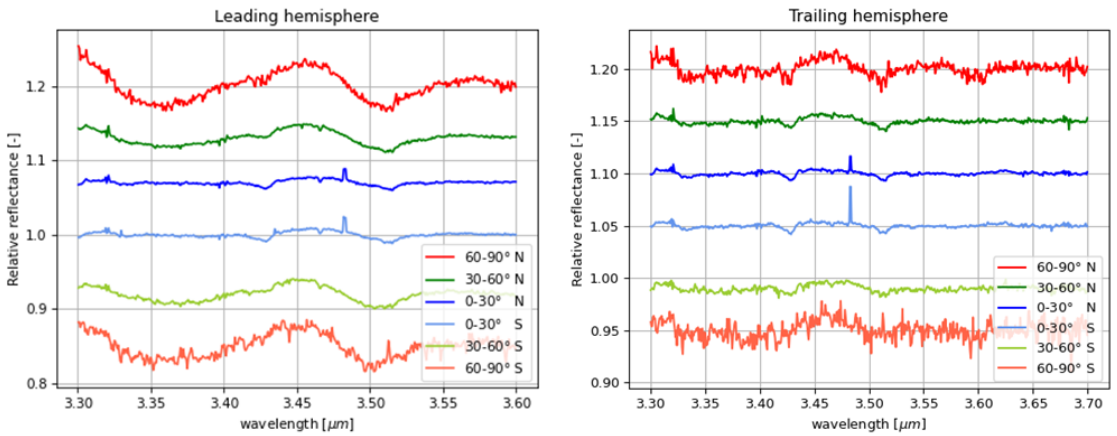

Figure B.12: Continuum subtracted spectra for the leading (left) and trailing (right) hemisphere for indicated latitudinal ranges. Note that the spectra are stacked for clarity and the y-axis is scaled according to the 0-30° N region.

Similar to the water ice and CO_2 features, maps of the equivalent width of the 3.42 band for both leading and trailing hemisphere are made and shown in figure B.13. Note that the equivalent width of the band is two orders of magnitude lower than that of water ice, confirming that the feature it is a faint feature. From the maps it is hard to distinguish a clear distribution. With some imagination, it can be said that the polar regions on the trailing hemisphere have a slight higher area than the equatorial region, but overall the distribution seems fairly homogeneous for both hemispheres. This makes it harder to interpret what the feature could be and how it originated.

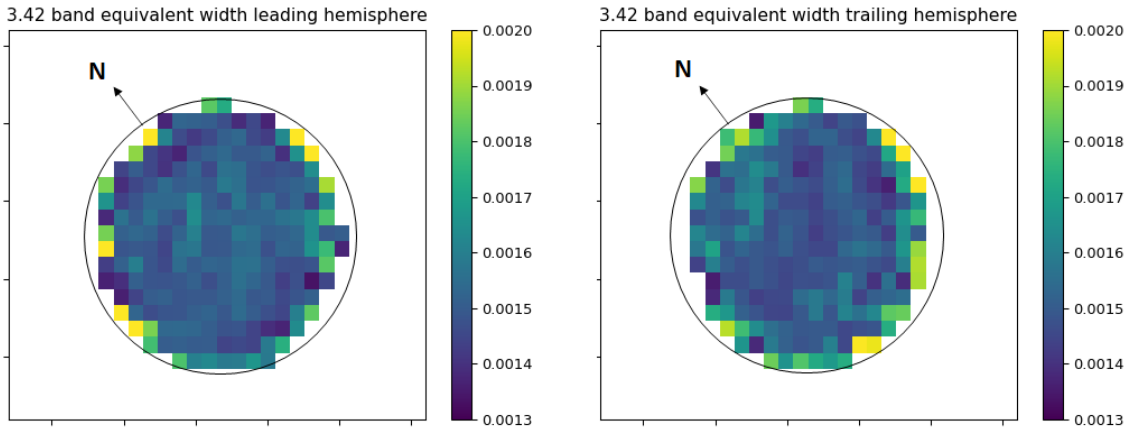

Figure B.13: Maps of the 3.42 band equivalent width for the leading (left) and trailing (right) hemisphere.

C

Validation

For any research it is important to validate results in order to be fully trustworthy. Therefore, this chapter will validate all the previous shown results. It will be presented in a similar way as the results chapter, thus starting with the data reduction in section C.1. Then the water ice results are validated in section C.2, after which CO_2 is discussed in section C.3. Finally, the results concerning organics will be validated in section C.4.

C.1. Data reduction

To validate the spectra, use is made of the Cubeviz visualisation tool [1] [2]. All JWST observations can be developed in this tool for quick-look analysis, which is shown in figure C.1. The bad pixels are not filtered out of the spectra and especially for the trailing hemisphere a lot of noise seems to be present. However, the overall shape of the spectra are similar to the ones produced in this work.

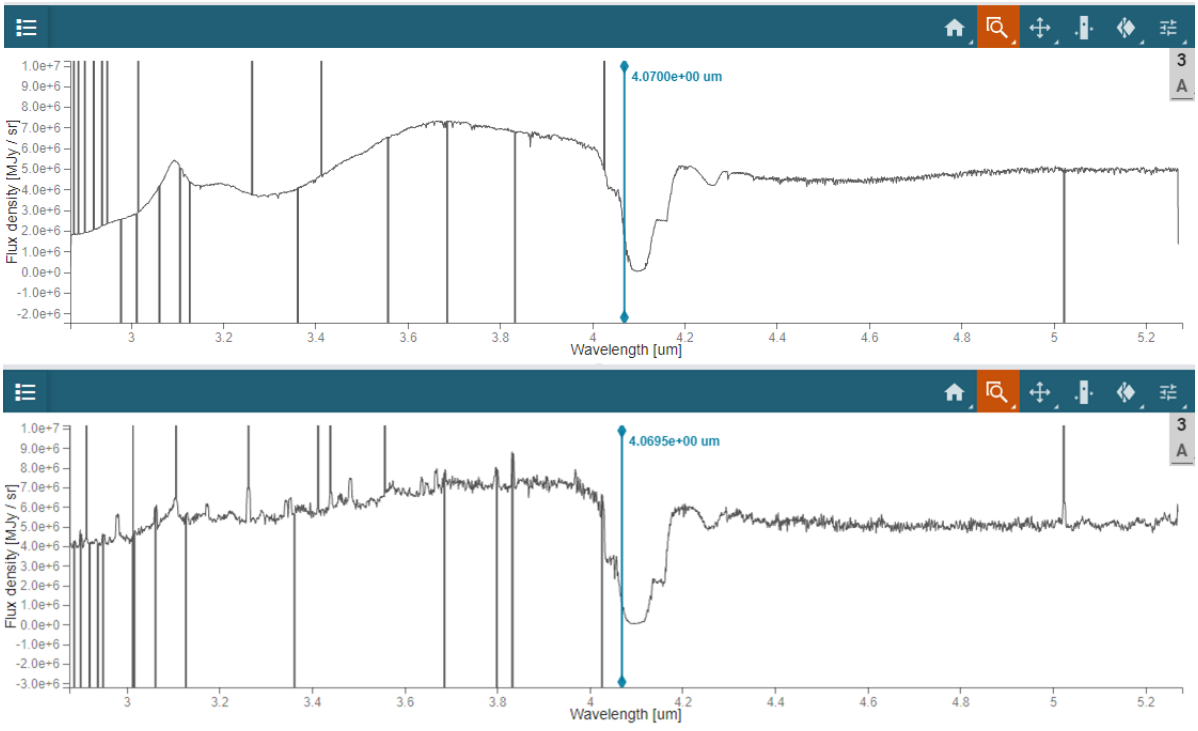

Figure C.1: Spectra of Ganymede's leading (top) and trailing (bottom) hemisphere using JWST's Cubeviz visualisation tool.

[1] https://mast.stsci.edu/viz/ui/#/spectra?filename=jw01373-o019_t001_nirspec_g395h-f290lp_s3d.fits
[2] https://mast.stsci.edu/viz/ui/#/spectra?filename=jw01373-o028_t001_nirspec_g395h-f290lp_s3d.fits

A second way to validate the JWST spectra is by looking at previous observations by the Galileo and Juno spacecraft. The spectra obtained in the two missions are shown in figure C.2. The spectra look very similar to the JWST spectra, having the same units and showing the same features. Therefore, it can be concluded that the spectra are properly developed.

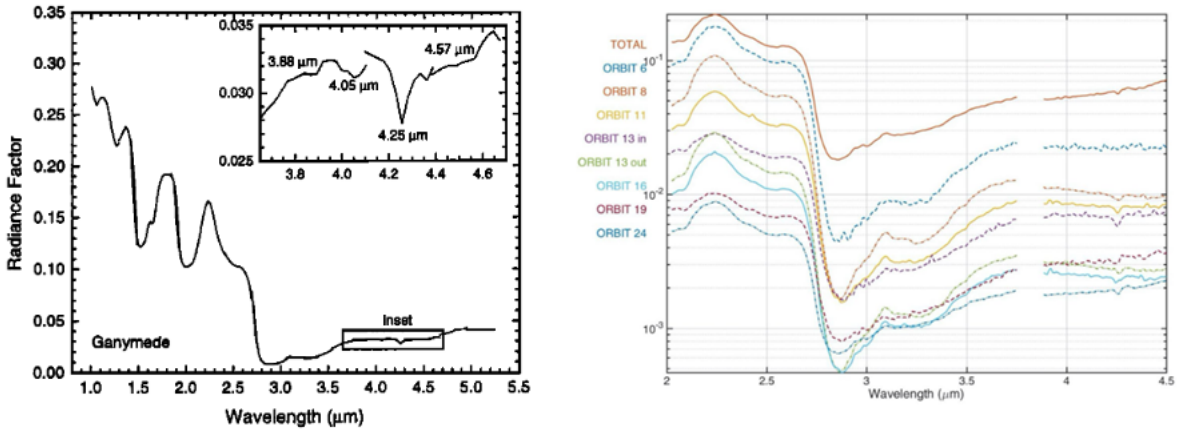

Figure C.2: Ganymede spectra of the NIMS instrument on board of the Galileo spacecraft (left) (McCord et al., 1998) and the JIRAM instrument on board of the Juno spacecraft (right) (Mura et al., 2020).

C.2. Water ice

Validating the distribution of water ice can be done by looking at other research into the water ice distribution on Ganymede. Trumbo et al. (2023) and Bockelée-Morvan et al. (in prep.) present the same Fresnel peak equivalent width distribution. Furthermore, water ice abundance on Ganymede was mapped prior to JWST observations as well, using ground based data based of the VLT. For this the 2 μm water band was used (Ligier et al., 2019). The resulting map is shown in figure C.3, where the right half represents the leading hemisphere and the left half represents the trailing. It can be deduced from the map that the obtained distribution is the same as the JWST observations, having more water ice on the leading hemisphere than on the trailing and overall more ice on the poles than around the equator.

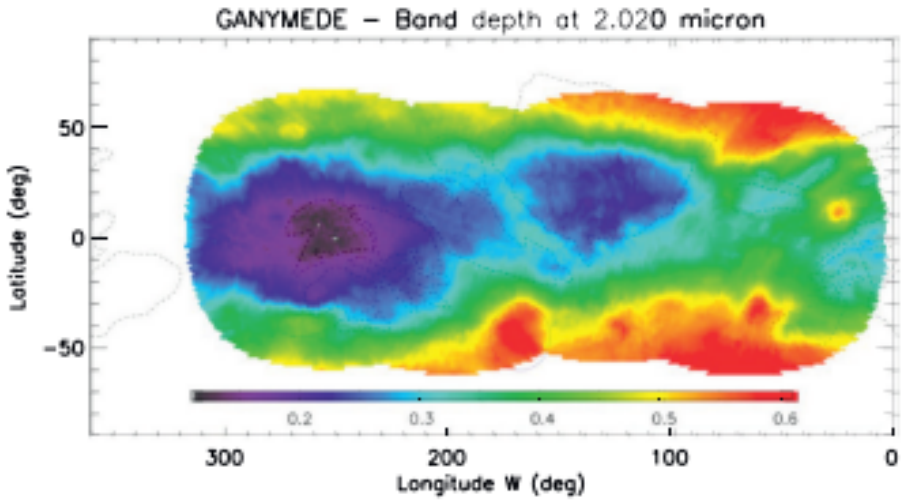

Figure C.3: Water ice abundance map of Ganymede using the 2 μm water band (Ligier et al., 2019). Note that the leading hemisphere is centred around 90°and the trailing hemisphere around 270°

C.3. CO_2

Previous research shows that on Ganymede and other Jovian and Saturnian icy moons in general, a blue-shift of the CO_2 band is common (Ahrens et al., 2022; Hibbitts et al., 2003). Therefore, it is no surprise that this shift occurs on Ganymede as well.

Compared to previous observations, some finding concerning CO_2 are found by the JWST observations as well. For example, Hibbitts et al. (2003) mentions symmetric behaviour of the CO_2 band depth for leading and trailing hemisphere. This was also found by the JWST observations. Furthermore, it is mentioned that there is little to no CO_2 present on the poles which agrees with the band depth maps in figure B.6. In the paper it is concluded that there is more CO_2 on bright terrains than on dark terrains. This correlation in albedo is not found with the JWST observations. For the leading hemisphere there is hardly a correlation between albedo and band depth, whereas on the trailing hemisphere there is a low band depth at high albedo (light) terrain, contradicting the findings of Hibbitts et al. (2003).

To summarise, the JWST observations agree with previous research in the latitudinal trend of CO_2 band depth and the symmetric behaviour of CO_2 for the leading and trailing hemisphere. The link with CO_2 abundance and terrain is not found with JWST observations. Nonetheless, since the JWST observes the entire disk of Ganymede in contrary to the Galileo spacecraft that was in orbit around Jupiter. Therefore, the overall distribution is easier to deduce from JWST observations making the findings reliable.

C.4. Organics

The results concerning organics are difficult to validate as there is not much previous research into the 3.42 μm band. Since the organics are not abundant, the feature appears weak in the reflectance spectra which makes it more challenging to analyse. However, the feature has been detected and mentioned in earlier research based on NIMS and JIRAM data (McCord et al., 1997; Pappalardo et al., 2004; Mura et al., 2020). This makes it trustworthy that the band is real even though it appears very shallow in the JWST spectra, having a band depth of only 1% maximum. To be fully convinced that the feature is not instrumental noise, the Ganymede spectra were compared to JWST observations of Io and G0V star P330-E, which is shown in figure C.4. From the figure it can be seen that the spectra of Io and P330-E contain more noise than the Ganymede spectrum. However, a clear absorption feature at 3.42 μm is not seen in the spectra. Therefore, it can be said with confidence that this band is no instrumental noise of NIRSpec's detector arrays.

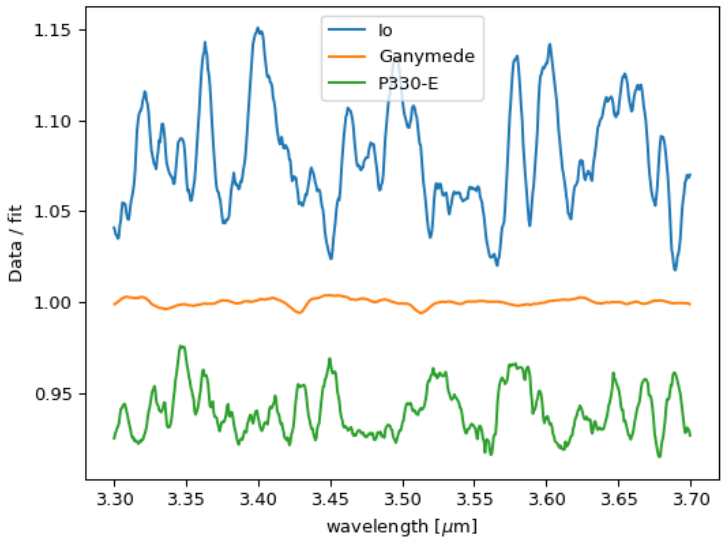

Figure C.4: Spectra of the 3.3-3.7 μm region of Io, Ganymede and star G0V P330-E (program 1538 (Gordon et al., 2022)) to compare the 3.42 μm feature.

The maps of the band area of the 3.42 μm feature were not conclusive, making it hard to validate whether they are reliable. However, the same method was used to reproduce the H_2O_2 maps presented by Trumbo et al. (2023). The H_2O_2 band has a similar band depth as the 3.42 μm feature, meaning that it could validate the method used. Figure C.5 shows the comparison of the H_2O_2 band with the results of Trumbo et al. (2023). The leading hemisphere is compared as there is hardly any H_2O_2 present on the trailing hemisphere.

From figure C.5, it can be seen that the distribution of the equivalent width is the same. Note that the orientation of the North pole is not the same. Near the limb, not all pixels represent the same area due to the usage of a different pipeline version. Furthermore, the spectra near the limb contain more noise, making it harder to obtain the true area for shallow features. Nonetheless, since the obtained distribution is the same, as well as the value of the area it is deemed that the method used to obtain the equivalent width of the 3.42 μm band is valid.

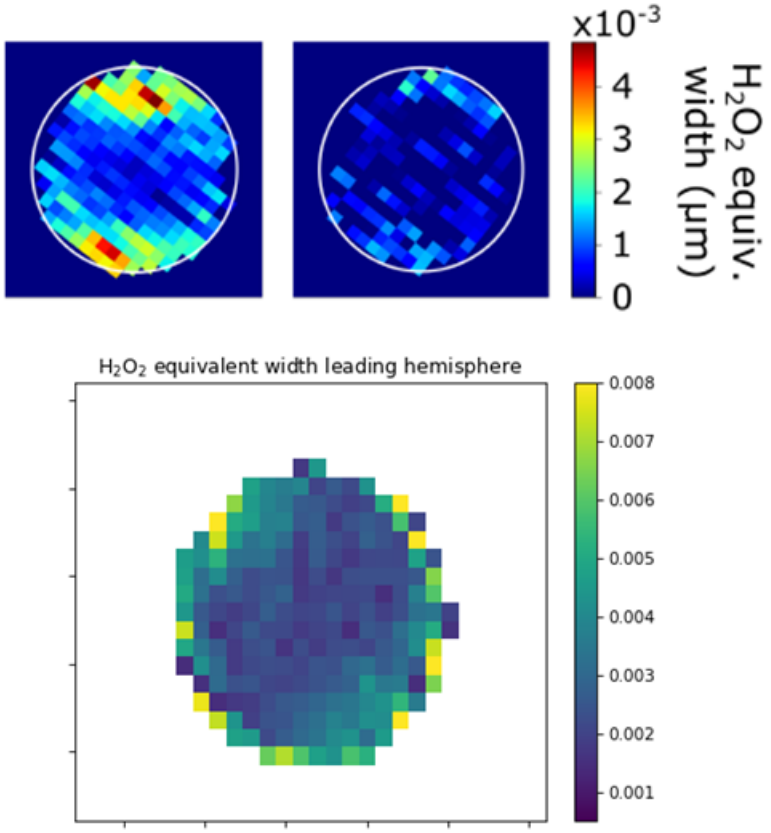

Figure C.5: Comparison with the H_2O_2 maps of Trumbo et al. (2023) to validate the method used for analysis of the 3.42 feature.

References

Ahrens, C., Meraviglia, H., and Bennett, C. (2022). A geoscientific review on co and co2 ices in the outer solar system. *Geosciences*, 12.

Anderson, J. et al. (1996). Gravitational constraints on the internal structure of ganymede. *Nature*, 384.

Berdis, J., Murphy, J., and Chanover, N. (2022). Europa's surface water-ice crystallinity and correlations between lineae and hydrate composition. *The Planetary Science Journal*, 3.

Clark, R. N., Cruikshank, D. P., Jaumann, R., Brown, R. H., Stephan, K., Dalle Ore, C. M., Eric Livo, K., Pearson, N., Curchin, J. M., Hoefen, T. M., Buratti, B. J., Filacchione, G., Baines, K. H., and Nicholson, P. D. (2012). The surface composition of iapetus: Mapping results from cassini vims. *Icarus*, 218(2):831–860.

De Kleer, K. et al. (2021). Ganymede's surface properties from millimeter and infrared thermal emission. *The Planetary Science Journal*.

Ehrenfreund, P., Kerkhof, O., Schutte, W., et al. (1999). Laboratory studies of thermally processed h2o-ch3oh-co2 ice mixtures and their astrophysical implications. *Astronomy and Astrophysics*, 350.

Gordon, K. et al. (2022). The james webb space telescope absolute flux calibration. i. program design and calibrator stars. *The Astronomical Journal*, 163.

Hansen, G. (2002). A method of measuring surface ice abundance: Application to ganymede. *Lunar and Planetary Science XXXIII*.

Hansen, G. and McCord, T. (2004). Amorphous and crystalline ice on the galileansatellites: A balance between thermal and radiolyticprocesses. *Journal of Geophysical Research*, 109.

He, J., Emtiaz, S., Boogert, A., and Vidali, G. (2018). The 12co2 and 13co2 absorption bands as tracers of the thermal history of interstellar icy grain mantles. *The Astrophysical Journal*, 869.

Hibbitts, C. A., Pappalardo, R. T., Hansen, G. B., and McCord, T. B. (2003). Carbon dioxide on ganymede. *Journal of Geophysical Research: Planets*, 108(E5).

Jones, B., Kaiser, R., and Strazzulla, G. (2014). Carbonic acid as a reserve of carbon dioxide on icy moons: The formation of carbon dioxide (co2) in a polar environment. *The Astrophysical Journal*, 788.

K. Isokoski, C. A. P. and Linnartz, H. (2013). Highly resolved infrared spectra of pure co2 ice (15–75 k). *Astronomy and Astrophysics*, 555.

Kay, J. and Head, J. (1999). Geologic mapping of the ganymede g8 calderas region: Evidence for cryovolcanism? *Lunar and Planetary Science*.

Kivelson, M. et al. (1996). Discovery of ganymede's magnetic field by the galileo spacecraft. *Nature*, 384.

Kivelson, M., Khurana, K., and Volwerk, M. (2002). The permanent and inductive magnetic moments of ganymede. *Icarus*, 157.

Leblanc, F. et al. (2017). On the orbital variability of ganymede's atmosphere. *Icarus*, 293.

Ligier, N. et al. (2019). Surface composition and properties of ganymede: Updates from ground-based observations with the near-infrared imaging spectrometer sinfoni/vlt/eso. *Icarus*, 333.

Mastrapa, R. et al. (2009). Optical constants of amorphous and crystalline h2o-ice: 2.5–22 μm (4000–455 cm−1) optical constants of h2o-ice. *The Astrophysical Journal*, 701.

McCord, T. et al. (1997). Organics and other molecules in the surfaces of callisto and ganymede. *SCIENCE*, 278.

McCord, T. et al. (1998). Non water ice constituents in the surface material of the icy galilean satellites from the galileo near-infrared mapping spectrometer investigation. *Journal Of Geophysical Research*, 103.

Merouane, S., Djouadi, Z., Le Sergeant d'Hendecourt, L., et al. (2014). Relations between aliphatics and silicate components in 12 stratospheric particles deduced from vibrational spectroscopy. *The Astrophysical Journal*, 780.

Mura, A. et al. (2020). Infrared observations of ganymede from the jovian infrared auroral mapper on juno. *AGU Advances*.

Pappalardo, R. et al. (2004). *Geology of Ganymede*. Cambridge University Press.

Patterson, G. et al. (2009). Global geological mapping of ganymede. *Icarus*, 207.

Pommerol, A. and Schmitt, B. (2008). Strength of the h2o near-infrared absorption bands in hydrated minerals: Effects of particle size and correlation with albedo. *Journal of Geophysical Research*, 113.

Prockter, L., Figueredo, P., et al. (2000). Geology and mapping of dark terrain on ganymede and implications for grooved terrain formation. *Journal of Geophysical Research*, 105.

Ravine, M. et al. (2022). Ganymede observations by junocam on juno perijove 34. *Geophysical Research Letters*, 49.

Schmitt, B. et al. (1998). Optical properties of ices from uv to infrared. *Solar System Ices*.

Stahler, S. and Palla, F. (2005). *The Formation of Stars*. John Wiley & Sons.

Stephan, K. et al. (2021). Vis-nir/swir spectral properties of h2o ice depending on particle size and surface temperature. *Minerals*, 1328.

Tielens, A. (2005). *The physics and chemistry of the interstellar medium*. Cambridge University Press.

Trumbo, S. K., Brown, M. E., Bockelée-Morvan, D., de Pater, I., and Fouchet, T. (2023). Hydrogen peroxide at the poles of ganymede. *Sciences Advances*.